(9) Spell et al. 1996
ERID # 55542

Cerro Toledo Rhyolite, Jemez Volcanic Field, New Mexico: $^{40}Ar/^{39}Ar$ geochronology of eruptions between two caldera-forming events

Terry L. Spell* — *Department of Geosciences, University of Houston, Houston, Texas 77204-5503 and Research School of Earth Sciences, Australian National University, Canberra ACT 0200, Australia*

Ian McDougall, **Anthony P. Doulgeris** — *Research School of Earth Sciences, Australian National University, Canberra ACT 0200, Australia*

ABSTRACT

The Cerro Toledo Rhyolite comprises a group of domes and tephra which were erupted during the interval between two caldera-forming ignimbrites, the Tshirege Member and Otowi Member of the Bandelier Tuff, in the Jemez Volcanic Field, New Mexico. To provide a chronologic framework for geochemical and isotopic studies on these rhyolites, which record the evolution of the Bandelier magma system during this interval, a $^{40}Ar/^{39}Ar$ geochronology study was undertaken. Pumice from major pyroclastic fall deposits within the rhyolite tephra and samples from the rhyolite domes were dated as well as the stratigraphically bracketing Bandelier Tuff. Analyzed crystal populations range from being fairly homogeneous juvenile material to very heterogeneous mixed juvenile and xenocrystic assemblages. In most cases dominant groups of juvenile sanidine crystals define $^{40}Ar/^{39}Ar$ ages which agree with stratigraphic constraints. Plagioclase analyses are distinctly more scattered and do not typically define reasonable ages. The $^{40}Ar/^{39}Ar$ ages for the two members of the Bandelier Tuff yield an interval of 387 ± 20 k.y. between these caldera-forming eruptions. During this interval nine major pyroclastic pumice units were deposited in the sections studied, for which six yield isochron ages, one a weighted mean age, one a maximum age, and one no reliable age due to lack of sanidine. $^{40}Ar/^{39}Ar$ dates on pumice fall units within the Cerro Toledo Rhyolite tephra indicate that eruptive activity occurred at >1.59, 1.54, 1.48, 1.37 and 1.22 Ma. $^{40}Ar/^{39}Ar$ dating of Cerro Toledo Rhyolite domes indicates these were erupted within the caldera at 1.54, 1.45, 1.38–1.34, and 1.27 Ma. The dates obtained indicate that eruptive activity occurred throughout the 380 k.y. interval between the two members of the Bandelier Tuff, but suggest that eruptions producing both tephra and domes occurred during discrete intervals at ca. 1.54, 1.48, and 1.38–1.34 Ma. The interval from 1.34 to 1.38 Ma was particularly active: 7 of 18 units dated are these ages.

INTRODUCTION

The mechanisms by which silicic magma chambers are generated and evolve continues to be debated (e.g., Smith, 1979; Hildreth, 1981; Lipman, 1984; Huppert and Sparks, 1988; Halliday et al., 1989; Christensen and DePaolo, 1993; Davies et al., 1994; Bogaard, 1995). Eruption triggering events, processes of crystallization within the magma chamber, and the longevity of large upper crustal magma chambers have been intensely studied, but are but not well understood. Multicyclic caldera systems in which the products of postcollapse volcanism are preserved provide the potential for studying these processes in detail. Voluminous ignimbrites record the characteristics of the magma chamber at an instant in time, whereas postcollapse volcanism records temporal evolution of the magma system and may yield insights into the transitions to and from these large eruptions and caldera collapse events. Good chronological constraints on, for example, rates of differentiation and timing of recharge events, are essential to the interpretation of geochemical and isotopic data from such systems.

The Valles-Toledo caldera complex, located near the center of the Jemez Volcanic Field (Fig. 1), provides an ideal opportunity for studying the evolution of silicic magma systems associated with multicyclic caldera complexes. This is because the products of two caldera-forming ignimbrite eruptions as well as postcollapse rhyolite domes and tephra are well preserved and exposed. In this study we examine the geochronology of the Cerro Toledo Rhyolite, a sequence of small-volume pyroclastic rocks and domes which were erupted during a 380 k.y. interval between two caldera-forming ignimbrites, the Otowi Member Bandelier Tuff (lower stratigraphic unit, ca. 1.61 Ma) and the Tshirege Member Bandelier Tuff (upper stratigraphic unit, ca. 1.23 Ma). These rocks thus record the evolution of the magma system from immediately following one caldera collapse event until immediately prior to the next caldera collapse event. Nine pumice fall units within the Cerro Toledo Rhyolite tephra, nine Cerro Toledo Rhyolite domes, and the bracketing Bandelier tuffs were dated by the single crystal laser fusion $^{40}Ar/^{39}Ar$ technique. These data form an integral part of a preliminary geochemical study (Spell et al., 1996) and will be critical to more detailed future work on the Bandelier silicic magma system.

GEOLOGIC OVERVIEW

The Jemez Volcanic Field is located in north-central New Mexico on the western margin of the Rio Grande rift (Fig. 1). The overall structure of the present-day volcanic field is dominated by basaltic to rhyolitic volcanic rocks of the Polvadera and Keres groups, which form the broad shield upon which younger silicic volcanic rocks of the Tewa Group were erupted (Bailey et al., 1969; Gardner and Goff, 1984; Gardner et al., 1986). Beginning at ca. 1.85 Ma a series of explosive rhyolitic eruptions occurred. The first of these produced the San Diego Canyon ignimbrites, which consist of two small (<10 km³) units (a stratigraphically lower unit A, and an upper unit B) that were vented from a source area beneath the Valles caldera (Self et al., 1986; Turbeville and Self, 1988; Spell et al., 1990). These were followed by the Bandelier tuffs, which represent ≈650 km³ of rhyolitic magma (Kuentz, 1986; Balsley, 1988). The Otowi Member was erupted 1.608 ± 0.010 Ma and resulted in collapse of the Toledo caldera.

*Present address: Spell, Department of Geosciences, University of Nevada, 4505 Maryland Parkway, Las Vegas, Nevada 89154

GSA Bulletin; December 1996; v. 108; no. 12; p. 1549–1566; 5 figures; 3 tables.

MAR 2 6 1997
em
14014

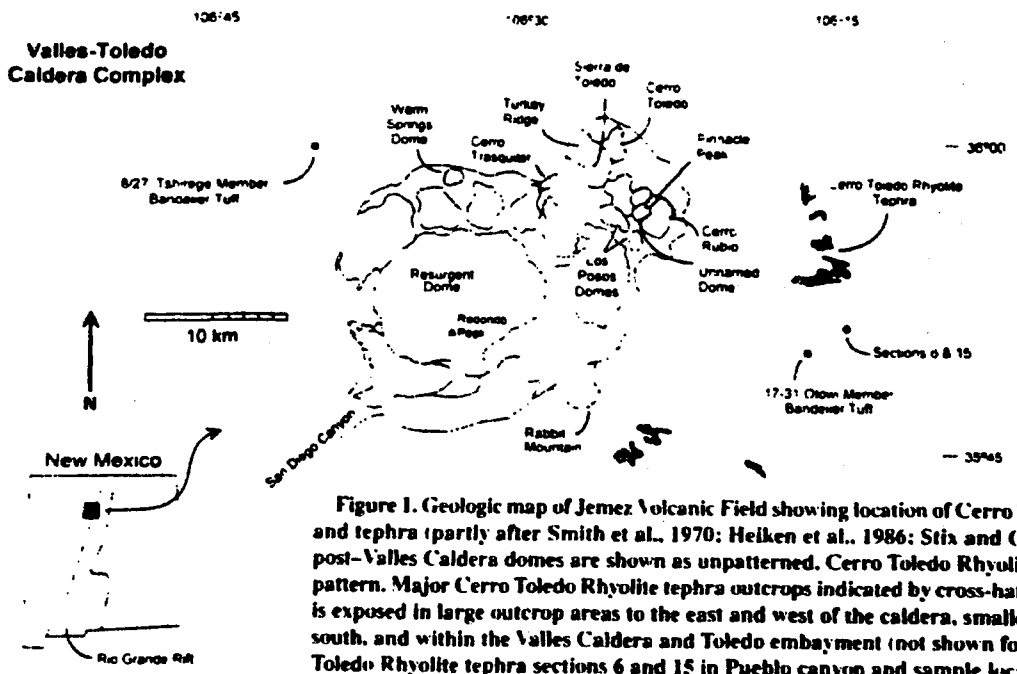

Figure 1. Geologic map of Jemez Volcanic Field showing location of Cerro Toledo rhyolite (CTR) domes and tephra (partly after Smith et al., 1970; Heiken et al., 1986; Stix and Gorton, 1993). Ring fracture post–Valles Caldera domes are shown as unpatterned. Cerro Toledo Rhyolite domes shown by speckled pattern. Major Cerro Toledo Rhyolite tephra outcrops indicated by cross-hatched pattern. Bandelier Tuff is exposed in large outcrop areas to the east and west of the caldera, smaller outcrops are to the north, south, and within the Valles Caldera and Toledo embayment (not shown for clarity). Location of Cerro Toledo Rhyolite tephra sections 6 and 15 in Pueblo canyon and sample localities for the Bandelier Tuff samples (Kuentz, 1986; Balsley, 1988) are indicated.

whereas the Tshirege Member, or upper Bandelier Tuff (Tshirege Member Bandelier Tuff), was erupted 1.225 ± 0.008 Ma and resulted in formation of the Valles caldera at a nearly coincident location (Smith and Bailey, 1968; Bailey et al., 1969; Heiken et al., 1986; Self et al., 1986). Rhyolite domes and associated tephra, the Cerro Toledo Rhyolite were erupted during the interval between the Otowi Member and the Tshirege Member (Griggs, 1964; Bailey et al., 1969). Preserved Cerro Toledo Rhyolite domes (some were likely destroyed during the collapse of the Valles caldera) are situated in the northeastern half of the Valles caldera and within the Toledo embayment, whereas the tephras are exposed in canyons to the east of the caldera (Fig. 1). Post-collapse rhyolites of the Valles caldera are included in the Valles Rhyolite Formation and consist dominantly of high-silica rhyolite domes and lavas (Griggs, 1964; Bailey et al., 1969; Spell and Kyle, 1989; Spell et al., 1993) which range in age from ca. 1.13 Ma to ca. 50–60 ka (Spell and Harrison, 1993; Reneau et al., 1996).

Previous Geochronology

The first K-Ar geochronology on rhyolites of the Valles caldera complex was reported by Doell and Dalrymple (1966) and the complete dataset was reported by Doell et al. (1968). Their work yielded ages of 1.12 ± 0.03 Ma for the Tshirege Member and 1.45 ± 0.06 Ma for the Otowi Member (all errors are quoted at the 1σ level; ages are adjusted, where necessary, to conform with the decay constants and isotopic abundances recommended by Steiger and Jäger, 1977) (Table 1).

$^{40}Ar/^{39}Ar$ dating of the Bandelier Tuff and San Diego Canyon ignimbrites was reported by Spell et al. (1990), who obtained ages of 1.14 ± 0.02 Ma (Tshirege Member), 1.51 ± 0.03 Ma (Otowi Member), and 1.78 ± 0.07 and 1.78 ± 0.04 Ma for San Diego Canyon ignimbrites A and B (lower and upper stratigraphic units), respectively. These ages were based on an age of 17.9 Ma for the Bern 4M muscovite standard from the interlaboratory calibration of Dalrymple and Lanphere (1971). In order to directly compare the $^{40}Ar/^{39}Ar$ ages of Spell et al. (1990) with those reported in this study they must be increased by 3.9% because Bern 4M has an age of 18.6 Ma relative to 27.9 Ma for the Fish Canyon Tuff sanidine standard used here (Hurford and Hammerschmidt, 1985). This yields ages of 1.19 ± 0.02 Ma, 1.57 ± 0.03 Ma, and 1.85 ± 0.07 Ma for the Tshirege Member, Otowi Member and San Diego Canyon ignimbrites, respectively. Izett and Obradovich (1994) reported $^{40}Ar/^{39}Ar$ ages on several Jemez rhyolites including the Tshirege Member and Otowi Member. They obtained weighted mean ages of 1.24 ± 0.02 Ma for the Tshirege Member and 1.63 ± 0.01 Ma for the Otowi Member (adjusted to an age of 27.9 Ma for the Fish Canyon Tuff sanidine standard).

A summary of published chronological data on the Cerro Toledo Rhyolite was given by Stix et al. (1988). Izett et al. (1981) reported K-Ar ages on a unit of the Cerro Toledo Rhyolite toward the middle of the section and on a unit near the top of the section of 1.47 ± 0.04 Ma and 1.23 ± 0.02 Ma, respectively (Table 1). Izett et al. also reported zircon fission track ages of 1.39 ± 0.06 and 1.46 ± 0.06 Ma for this sample. Stix et al. (1988) reported a K-Ar age of 1.52 ± 0.04 Ma on a sample from stratigraphic level 27 (Table 1). Additional age data, summarized by Stix et al. (1988), from rhyolite domes of the Cerro Toledo Rhyolite that may provide chronological ties with the tephras are discussed below.

A stratigraphic chronology based on the K-Ar age data from Cerro Toledo Rhyolite tephra is in Table 1. The data suggest that more than half of the Cerro Toledo Rhyolite tephra stratigraphic sequence in the sections studied was erupted ca. 1.5 Ma: the K-Ar age for the Otowi Member and stratigraphic levels 22 and 27 (near the middle of the sequence) are indistinguishable at the 2σ level. An apparent hiatus of ca. 290 k.y. appears between level 22 and the next dated horizon, level 41, which has an age indistinguishable from the K-Ar age of the Tshirege Member.

METHODS AND DATA TREATMENT

Nine Plinian pumice fall units within the Cerro Toledo Rhyolite tephra and nine Cerro

TABLE 1. STRATIGRAPHIC RELATIONS AND GEOCHRONOLOGY OF CERRO TOLEDO RHYOLITE TEPHRA AND ASSOCIATED UNITS

Stratigraphic level*	Section 6*	Section 15*	Sample ID	K/Ar (Ma ± σ)	$^{40}Ar/^{39}Ar$ (Ma ± σ) Isochron	Mean	Weighted mean
45	—	—	8/27 (TM)	1.12 ± 0.03†	1.225 ± 0.008§	1.220 ± 0.007	1.212 ± 0.006
44	6-11	—					
43	—	—					
42	6-10	—					
41	6-8	—	CT-9	1.23 ± 0.02#	1.212 ± 0.009§	1.213 ± 0.010	1.212 ± 0.007
38	—	15-6	CT-6	—	1.362 ± 0.016§	1.404 ± 0.124	1.389 ± 0.011
35	—	15-12	CT-5	—	1.376 ± 0.018§	1.387 ± 0.012	1.384 ± 0.008
34	—	15-7					
33	—	15-11					
30	6-6	—					
27	6-5	—	CT-8	1.52 ± 0.04**	1.479 ± 0.020§	1.457 ± 0.016	1.459 ± 0.008
26	6-4	—					
23	6-4	—					
22	6-3	—	CT-7	1.47 ± 0.04#	N.D.O. (s)	1.543 ± 0.066 (s)	1.520 ± 0.016 (s)
					N.D.O. (p)	1.324 ± 0.215 (p)	1.205 ± 0.024 (p)
	—	—	CT-4	—	1.474 ± 0.023§ (s)	1.488 ± 0.024 (s)	1.491 ± 0.009 (s)
					N.D.O (p)	1.370 ± 0.143 (p)	1.287 ± 0.019 (p)
21	6-2	—					
18	6-1	15-10	CT-3	—	1.451 ± 0.022	1.531 ± 0.032	1.542 ± 0.008§
15	—	15-5					
14	—	15-9	CT-2	—	1.536 ± 0.018§	1.558 ± 0.033	1.550 ± 0.008
11	—	15-8					
10	—	15-8					
9	—	15-8					
8	—	15-8	CT-1	—	N.D.O.	1.653 ± 0.032	1.652 ± 0.008
7	—	15-8					
6	—	—					
5	—	—					
2	—	—	17-31 (OM)	1.45 ± 0.06†#	1.608 ± 0.010§	1.611 ± 0.008	1.609 ± 0.008

Notes: Australian National University data. N.D.O. = no date obtained. TM = Tshirege Member Bandelier Tuff. OM = Otowi Member Bandelier Tuff. Isochron ages calculated using inverse isochron York (1969) fit routine and omitting outliers until MSWD < 2.5. errors include J and MSWD. Weighted mean ages use weighting by the inverse of the variance, errors include 0.5% J factor error. All ages are sample mean ± population standard deviations. Means and weighted means are calculated using model apparent ages and exclude analyses >2σ from the mean. All $^{40}Ar/^{39}Ar$ analyses are sanidine unless otherwise indicated. For samples where both sanidine and plagioclase were analyzed. s = sanidine, p = plagioclase

*Stratigraphic levels and section unit numbers from Stix (1989)

†Doell et al. (1968).

§Preferred ages.

#Izett et al. (1981).

**Stix et al. (1988)

Toledo Rhyolite domes within the Valles-Toledo caldera complex were sampled (Fig. 1, Tables 1 and 2). The pumice-fall samples were collected from two sections (6 and 15, located 1.2 km apart in Pueblo Canyon) in order to sample the complete Cerro Toledo Rhyolite stratigraphy between the two members of the Bandelier Tuff and are considered to represent the most significant eruptive events preserved within this sequence (i.e., the onset of an eruption within the caldera). The Cerro Toledo Rhyolite tephra consists of Plinian pumice fall units, phreatomagmatic fall and surge ash beds, and epiclastic sedimentary rocks (Stix et al., 1988). The tephra are dominantly phenocryst poor, containing <5% crystals; the major phases are quartz and sanidine, and plagioclase is usually constituting a minor phase (Stix et al., 1988). Most units contain separable amounts of sanidine, and this was the primary phase analyzed. For units where sanidine was sparse, both sanidine and plagioclase were analyzed. Dome samples range from nearly aphyric to phenocryst rich (≈25%); most have ≈5%–10% phenocrysts. Cerro Toledo Rhyolite tephra samples were dated at the Australian National University; and dome samples were dated at the University of Houston. Analytical procedures are discussed separately below.

Mineral separates were prepared at the Australian National University. Unaltered pumice clasts (≈1 to ≈5 cm) were wire brushed to remove surface material and then crushed. Approximately 10–30 clasts were used for each separate. Whole-rock samples were crushed and sieved. Sanidine and plagioclase were obtained by standard heavy liquid techniques followed by hand picking, and were ultrasonically treated in dilute HF (7%) for 10 min to remove adhering glass. Separated crystals ranged in size from ≈0.5 to 2 mm and weighed from ≈0.5 to 5 mg.

Australian National University Laboratory Methods

Samples analyzed at the Australian National University were wrapped in Sn foil and stacked in a silica tube for irradiation. Samples were alternated with fluence monitors (standard minerals), 92–176 sanidine (separated from the Fish Canyon Tuff), such that ≈5 mm separated fluence monitor positions. Loaded silica tubes were packed in an Al irradiation container lined with 0.2-mm-thick Cd for shielding against thermal neutrons. Synthetic K-bearing glass (obtained from B. Turrin, U.S. Geological Survey) and optical grade CaF_2 were included in the irradiation packages to monitor neutron induced argon interferences from K and Ca. Irradiations (20 h) done in the X33 or X34 positions adjacent to the core of the HIFAR nuclear reactor at Lucas Heights, New South Wales. Sample containers were inverted three times during the irradiations in order to reduce neutron fluence gradients in both the horizontal and vertical dimensions. Correction factors determined by repeated isotopic analysis of irradiated K glass and CaF_2 fragments were: $(^{40}Ar/^{39}Ar)_K = 2.57 (\pm 0.19) \times 10^{-2}$ (irradiation can K798/181) and $1.84 (\pm 0.26) \times 10^{-2}$ (irradiation can K746/182), $(^{36}Ar/^{37}Ar)_{Ca} = 3.50 (\pm 0.14) \times 10^{-4}$ and $(^{39}Ar/^{37}Ar)_{Ca} = 7.86 (\pm 0.01) \times 10^{-4}$. J factors were determined by laser fusions of 4–5 single crystals (≈0.2 mg) of the Fish Canyon Tuff sanidine standard, which yielded reproducibility of 0.11% to 0.45% (standard deviation of population) at each level, within the range of mass spectrometer analytical errors for individual analyses. An error in J of 0.5% was used in age calculations. Variation in

TABLE 2. GEOCHRONOLOGY OF CERRO TOLEDO RHYOLITE DOMES AND ASSOCIATED UNITS

Sample ID	Dome	K/Ar (Ma ± σ)	$^{40}Ar/^{39}Ar$ (Ma ± σ)		
			Isochron	Mean	Weighted mean
WS-2	Warm Springs	1.25 ± 0.04*	1.265 ± 0.011†	1.267 ± 0.025	1.263 ± 0.011
TE-9	Sierra de Toledo	—	1.336 ± 0.018†	1.326 ± 0.027	1.336 ± 0.012
TE-15	Turkey Ridge	1.24 ± 0.03*	1.343 ± 0.015†	1.351 ± 0.026	1.348 ± 0.021
TE-1	Unnamed dome	1.33 ± 0.02§	1.348 ± 0.010†	1.356 ± 0.013	1.357 ± 0.011
TE-26	Cerro Trasquilar	1.27 ± 0.02*	1.359 ± 0.012†	1.368 ± 0.048	1.369 ± 0.011
TE-13	Sierra de Toledo	—	1.379 ± 0.012†	1.367 ± 0.030	1.380 ± 0.011
TE-20	Los Posos East	1.47 ± 0.05*	1.446 ± 0.009†	1.481 ± 0.027	1.477 ± 0.009
TE-18	Indian Point	—	1.463 ± 0.011†	1.457 ± 0.018	1.464 ± 0.009
TE-25	Los Posos West	1.50 ± 0.05*	1.540 ± 0.012†	1.548 ± 0.018	1.545 ± 0.016
17-31 BT	Otowi Member	1.45 ± 0.06#	1.618 ± 0.011†	1.644 ± 0.053	1.625 ± 0.009

Notes. University of Houston data. Isochron ages calculated using inverse isochron York (1969) fit routine and omitting outliers until MSWD < 2.5. errors include J and MSWD. Weighted mean ages use weighting by the inverse of the variance, errors include 0.5% J factor error. Mean ages are sample mean ± population standard deviations. Means and weighted means are calculated using model apparent ages and exclude analyses greater than 2σ from the mean. BT, Bandelier Tuff. All $^{40}Ar/^{39}Ar$ analyses are on sanidine.

*Stix et al. (1988)
†Preferred ages.
§Doell et al. (1968)
#Izett et al. (1981)

neutron fluence along the 31 mm length of the Si irradiation tubes was <3%. The excellent reproducibility of the single crystal fluence monitor fusions indicates that no significant neutron flux gradients were present within individual packets of crystals.

Irradiated crystals, together with CaF_2 and K glass fragments, were placed in a Cu sample tray within an ultrahigh vacuum extraction line and fused using a 10 W Ar ion laser. A binocular microscope and a video camera system was used to view samples during fusion. Reactive gases were removed by a 10 L s^{-1} SAES getter prior to being admitted to a VG3600 mass spectrometer by expansion. The relative volumes of the extraction line and mass spectrometer allowed ≈82% of the gas to be admitted to the mass spectrometer. Peak intensities were measured using a Daly photomultiplier collector system by peak hopping through seven cycles; initial peak heights were determined by linear regression to the time of gas admission. Mass spectrometer discrimination and sensitivity was monitored by repeated analysis of atmospheric argon aliquots from an on-line air argon pipette system. Measured $^{40}Ar/^{36}Ar$ ratios were 289.9 ± 0.6 (1σ), and the appropriate discrimination corrections of 1.00458 to 1.00507 (1 AMU) were applied to isotope ratios. The measured sensitivity of the mass spectrometer was ≈1.25×10^{-17} mol mV^{-1}. Line blanks were checked after each 3–5 analyses; they averaged 2.5×10^{-16} mol for mass 40 and were undetectable at mass 36. Mass spectrometer backgrounds were measured before each analysis and the appropriate corrections made to subsequent data. Discrimination, sensitivity, blanks, and backgrounds were relatively constant over the period of data collection. Final data reduction and age calculations were done using Macintosh-based software (KArDate) written at the Australian National University. An age of 27.9 Ma (Steven et al., 1967; Cebula et al., 1986) was used for the Fish Canyon Tuff sanidine fluence monitor in calculating ages for samples.

University of Houston Laboratory Methods

Samples analyzed at the University of Houston were wrapped in Al foil and stacked in a 6-mm-inside-diameter Pyrex tube. Individual packets averaged 3 mm thick and fluence monitors (Australian National University 92-176, Fish Canyon Tuff sanidine) were placed approximately every 6 mm along the tube. Loaded silica tubes were packed in an Al container for irradiation. Synthetic K-bearing glass (obtained from B. Turrin, U.S. Geological Survey) and optical grade CaF_2 were included in the irradiation packages to monitor neutron induced argon interferences from K and Ca. Samples were irradiated for 5 h in the D3 position on the core edge (fuel rods on three sides, moderator on the fourth side) of the 1MW TRIGA type reactor at the Nuclear Science Center of Texas A&M University. Irradiations are performed in a dry tube device, shielded against thermal neutrons by a 5 mm thick jacket of B_4C powder, which rotates about its axis at a rate of 0.7 rpm to mitigate horizontal flux gradients. Correction factors for interfering neutron reactions on K and Ca were determined by repeated analysis of K glass and CaF_2 fragments. Measured $(^{40}Ar/^{39}Ar)_K$ values were <0.00012, always within 1σ of 0, thus no correction for the $^{40}K(n,p)^{40}Ar$ reaction was made. Ca correction factors were $(^{36}Ar/^{37}Ar)_{Ca}$ = 2.75 (± 0.06) × 10^{-4} and $(^{39}Ar/^{37}Ar)_{Ca}$ = 6.82 (± 0.34) × 10^{-4}. J factors were determined by fusion of 3–5 individual crystals of 92-176 sanidine (Fish Canyon Tuff sanidine), which gave reproducibilities of 0.15% to 0.20% (1 s.d.) at each standard position. Variation in neutron flux along the 80 mm length of the Si irradiation tubes was <7%. An error in J of 0.5% was used in age calculations. No significant neutron flux gradients were present within individual packets of crystals, as indicated by the excellent reproducibility of the single crystal fluence monitor fusions.

Irradiated crystals together with CaF_2 and K glass fragments were placed in a Cu sample tray in an ultrahigh vacuum extraction line and were fused using a 10 W CO_2 laser. Samples were viewed during fusion by a video camera system, and were positioned on a motorized sample stage. Reactive gases were removed by a 50 L s^{-1} SAES getter prior to being admitted to a MAP 215–50 mass spectrometer by expansion. The relative volumes of the extraction line and mass spectrometer allow ≈80% of the gas to be admitted to the mass spectrometer. Peak intensities were measured using a Johnston electron multiplier by peak hopping through seven cycles; initial peak heights were determined by linear regression to the time of gas admission. Mass spectrometer discrimination and sensitivity were monitored by repeated analysis of atmospheric argon aliquots from an on-line pipette system. Measured $^{40}Ar/^{36}Ar$ ratios were 292.9 ± 1.7 (1σ); thus discrimination corrections of 1.00085 to 1.00369 (1 AMU) were applied to measured isotope ratios. The sensitivity of the mass spectrometer was ≈1.6×10^{-17} mol mV^{-1}. Line blanks were checked after each 3 analyses and averaged 1.2×10^{-16} mol for mass 40 and 2.4×10^{-18} mol for mass 36. Discrimination, sensitivity, and blanks were relatively constant over the period of data collection. Computer-automated operation of the sample stage, laser, extraction line, and mass spectrometer as well as final data reduction and age calculations were done using Macintosh-based software written by A. Deino (University of California, Berkeley). An age of 27.9 Ma (Steven et al., 1967; Cebula et al., 1986) was used for the Fish Canyon Tuff sanidine fluence monitor in calculating ages for samples.

Intercalibration of the $^{40}Ar/^{39}Ar$ dating Laboratories

Intercalibration of the Australian National University $^{40}Ar/^{39}Ar$ data with those from the University of Houston was accomplished by analyzing sample 17-31 (Otowi Member, Bandelier Tuff) at both laboratories. The fluence monitor for samples run in both labs was 92-176, which is 27.9 Ma sanidine from the Fish Canyon Tuff (Steven et al., 1967; Cebula et al., 1986). That identical results were obtained for the age of sample 17-31 (see below) indicates that the two datasets are directly comparable.

Data Treatment

A major advantage of dating individual crystals from explosively erupted volcanic rocks is that mixed crystal populations consisting of ju-

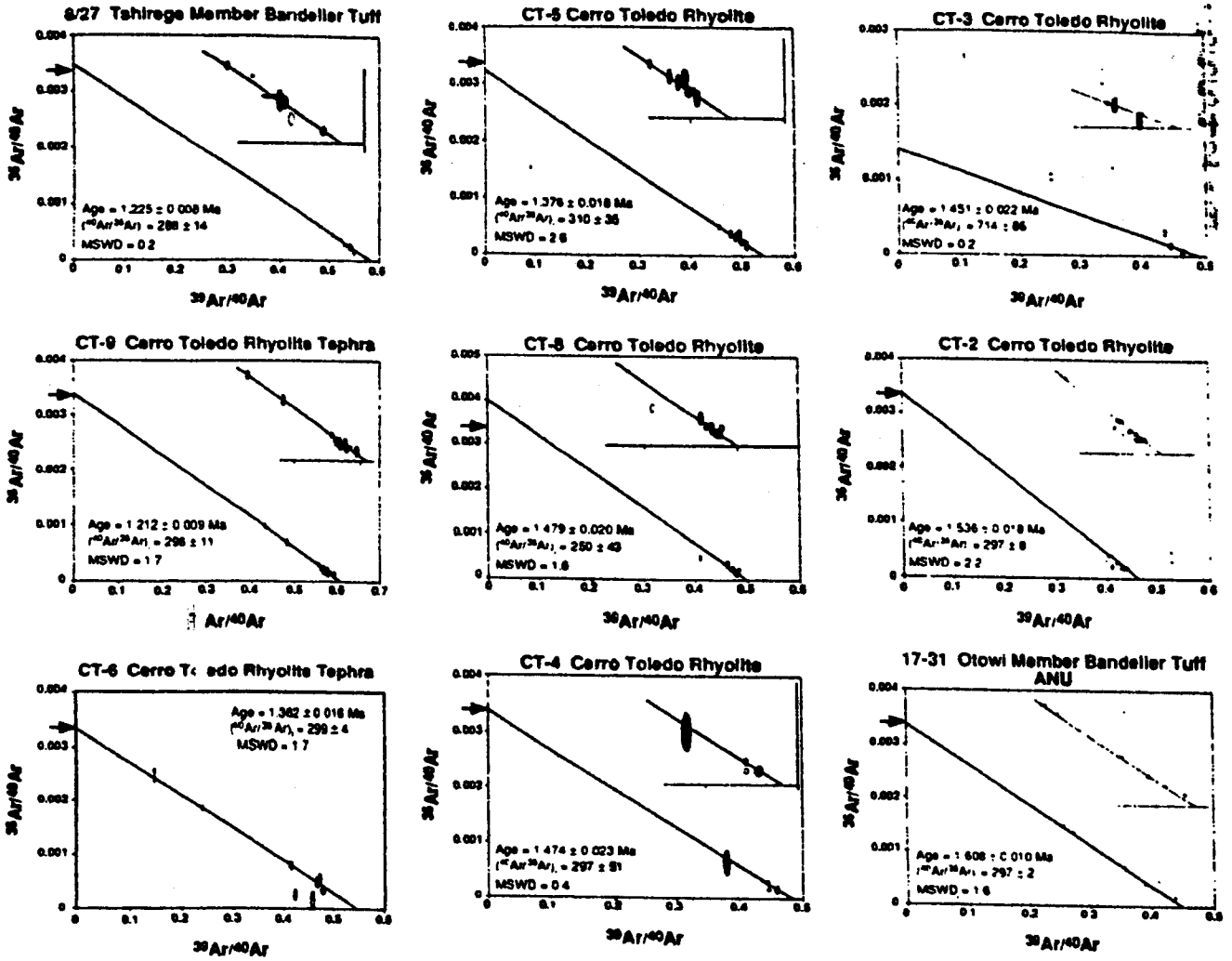

Figure 2 (Above and on following pages). Isochron plots for single crystal $^{40}Ar/^{39}Ar$ analyses of the Otowi Member, Tshirege Member, and Cerro Toledo Rhyolite samples. Analyses defining the isochron are shown by solid symbols whereas those omitted are shown by open symbols. Error ellipses are shown at 2σ. Arrows on $^{36}Ar/^{40}Ar$ axis indicate composition of atmospheric argon. Note that sample 17-31 (Otowi Member) was analyzed at both the Australian National University (ANU) and the University of Houston (UofH).

venile phenocrysts, altered crystals, and xenocrysts can be identified. Ideally this will allow an accurate eruptive age to be calculated based on the ages of juvenile phenocrysts alone, provided that they can be unambiguously identified. Two methods are used here to assess the homogeneity of analyzed crystal populations and to identify juvenile phenocrysts. First, sample means and population standard deviations are calculated. Any samples greater than 2σ from the mean are excluded and a new mean calculated. Weighted means of these refined datasets are also calculated using the inverse of the variance as the weighting factor (Young, 1962). Weighted mean ages are initially calculated using analytical errors only and a 0.5% J factor error is then incorporated by quadratically combining it with the weighted standard error. Second, isochron ages are calculated using a method outlined previously (Deino and Potts, 1990; Spell and Harrison, 1993). All analyses are regressed on an isochron using the York (1969) routine. If mean square of weighted deviates (MSWD) is greater than ≈2.5 (indicating geologic scatter in the data as might be caused by the presence of xenocrysts) the analysis contributing the most to the MSWD is omitted and the remaining data regressed again. This process is repeated if necessary, and the result is monitored visually by use of a frequency distribution diagram, until a homogeneous crystal population is defined. In some cases MSWD falls from above 2.5 to below 1 upon omission of the last outlier. For MSWD less than 1, the standard interpretation is that the analytical errors have been overestimated. In the cases we find here it is most likely the result of having a very homogeneous population of analyses from small crystals, resulting in relatively large errors on each analysis. For samples that define acceptable isochrons, the age and error quoted includes the 0.5% error in J as well as an additional square root of MSWD error to account for scatter in the dataset.

Analyzed crystal populations typically consist of a dominant group of juvenile phenocrysts,

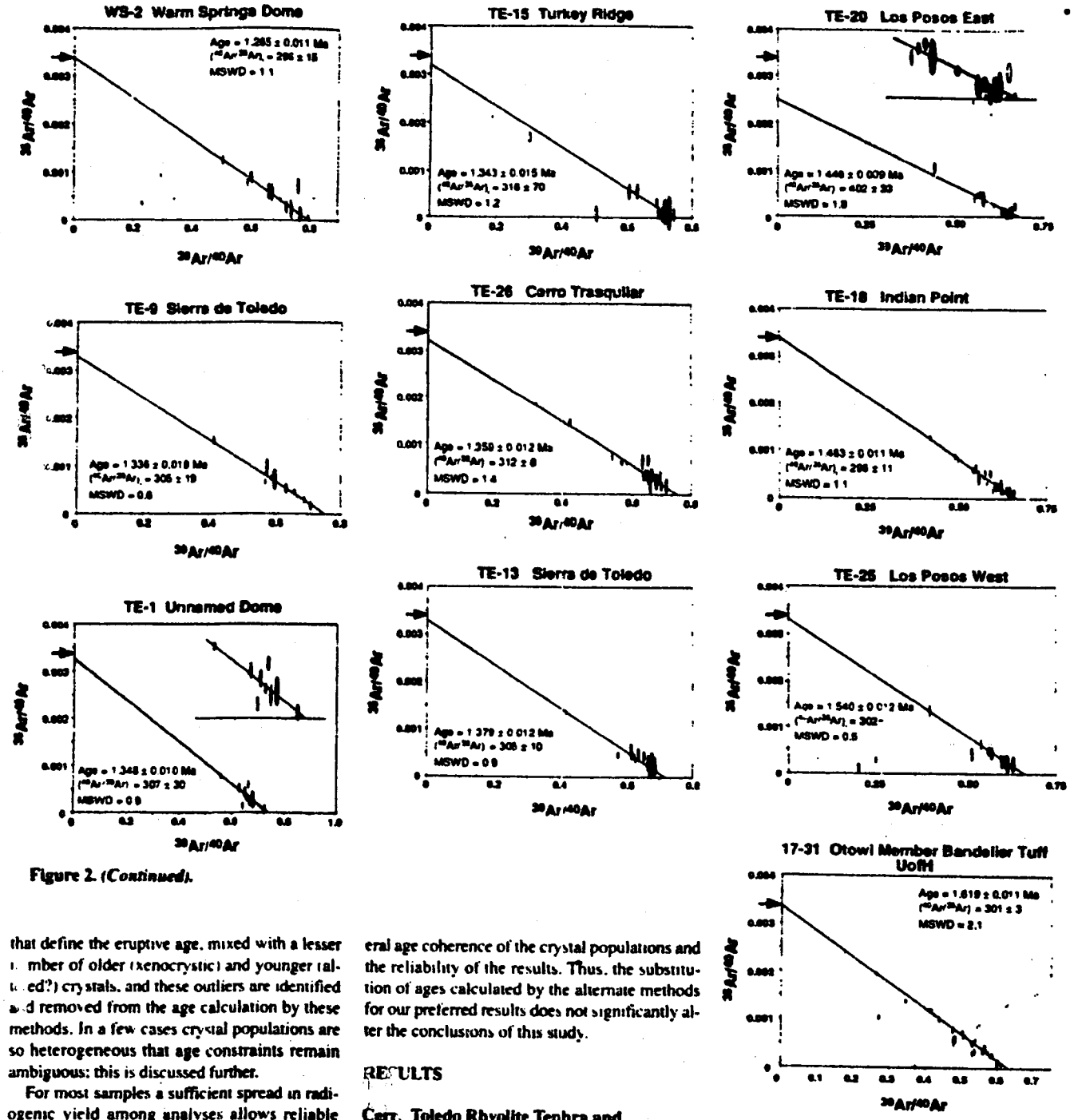

Figure 2. *(Continued).*

that define the eruptive age, mixed with a lesser number of older (xenocrystic) and younger (altered?) crystals, and these outliers are identified and removed from the age calculation by these methods. In a few cases crystal populations are so heterogeneous that age constraints remain ambiguous; this is discussed further.

For most samples a sufficient spread in radiogenic yield among analyses allows reliable isochrons to be defined, and these are taken as giving the preferred age of the unit (see Table 1). For a few samples the weighted mean age is preferred; these are pointed out in the next section. We emphasize that in some cases these methods of calculating an age result in rejection of different analyses; however, the overall agreement in ages by the different methods illustrates the general age coherence of the crystal populations and the reliability of the results. Thus, the substitution of ages calculated by the alternate methods for our preferred results does not significantly alter the conclusions of this study.

RESULTS

Cerro Toledo Rhyolite Tephra and Bandelier Tuff—Australian National University Data

Eight fusions of sanidine crystals from the Tshirege Member of the Bandelier Tuff gave a very homogeneous population of six crystals at ca. 1.22 Ma, and a total range in ages from 1.206 to 1.247 Ma (Table 3). The isochron analysis results in exclusion of two outliers (samples 8/27-6a and 8/27-7a) and yields an age of 1.225 ± 0.008 Ma, an initial $^{40}Ar/^{36}Ar$ of 288.3 ± 13.9, and a mean square of weighted deviates (MSWD) of 0.2 (Figs. 2 and 3, Table 1). The mean and weighted mean analysis results in exclusion of 8/27-7a and gives similar results of

1.220 ± 0.007 Ma and 1.212 ± 0.006 Ma, respectively (Table 1).

Eight fusions of sanidine crystals from the middle flow unit of the Otowi Member of the Bandelier Tuff (sample 17-31) yield apparent ages from 1.580 to 1.623 Ma (Table 3). The isochron approach yields an age of 1.608 ± 0.010 Ma, initial $^{40}Ar/^{36}Ar$ of 296.6 ± 2.2, and a MSWD of 1.6 (Figs. 1 and 2) after omitting 1731-5a (Table 1). The mean omits the same analysis and gives an age of 1.611 ± 0.008 Ma and the corresponding weighted mean is 1.609 ± 0.008 Ma (Table 1). These three ages are indistinguishable emphasizing the homogenous ages of the analyzed crystal population.

Sample 92-CC-01 is from the Otowi Member ignimbrite exposed in a complexly channeled outcrop in Cochiti Canyon (J. A. Wolff, 1994, personal commun.). A population of eight analyzed sanidine crystals is heterogeneous, having apparent ages of 1.566 to 1.690 Ma (Table 3). An isochron regressed using all the data yields an age of 1.604 ± 0.049 Ma with a MSWD of 35.6. Exclusion of three outliers (Fig. 3) results in an isochron age of 1.601 ± 0.014 Ma, initial $^{40}Ar/^{36}Ar$ of 296.7 ± 2.2, and an acceptable MSWD of 2.6 (not shown). The mean age is 1.620 ± 0.042 Ma with no excluded data and the weighted mean is 1.601 ± 0.014 Ma. These ages are indistinguishable from that of the Otowi Member middle flow unit (see above).

Sample CT-9 yielded a very homogeneous population of sanidine apparent ages averaging ≈1.21 Ma (Fig. 3, Table 3). The 10 analyses fall on an isochron that defines an age of 1.212 ± 0.009 Ma, an initial $^{40}Ar/^{36}Ar$ of 295.5 ± 10.6, and a MSWD of 1.7 (Fig. 2). The mean and weighted mean ages of 1.213 ± 0.010 Ma and 1.212 ± 0.007 Ma, respectively, are virtually identical (Table 1) and also include all analyses.

Nine sanidine crystals from sample CT-6 define a dominant group at ≈1.37 Ma (Table 3). The isochron treatment results in omitting two distinctly older outliers (CT6-5a and CT6-7a) and one younger outlier (CT6-8a). This gives a six-point isochron and an age of 1.362 ± 0.016 Ma, an initial $^{40}Ar/^{36}Ar$ of 298.8 ± 3.8, and a MSWD of 1.7 (Figs. 2 and 3). No omissions are indicated for the mean age of 1.404 ± 0.124 Ma, and the corresponding weighted mean is 1.389 ± 0.011 Ma (Table 1). These three age estimates overlap at the 1σ level.

Ten fusions of sanidine crystals from CT-5 yielded a fairly homogeneous population with a mean of 1.383 Ma (Tables 1 and 3). An isochron regressed using all the data yields an age of 1.376 ± 0.018 Ma, an initial $^{40}Ar/^{36}Ar$ of 310.6 ± 35.1, and a MSWD of 2.6 (Figs. 2 and 3). Although slightly above the 2.5 MSWD cutoff level, this result is deemed acceptable because the MSWD for the standard isochron ($^{39}Ar/^{36}Ar$ vs. $^{40}Ar/^{36}Ar$) is 1.7. The mean age indicates exclusion of sample CT5-5a and gives an age of 1.387 ± 0.012 Ma. The weighted mean of these data is 1.384 ± 0.008 Ma (Table 1). These three estimates of the age are virtually identical and emphasize the age coherence of the analyses.

Ten fusions of sanidine crystals from CT-8 yielded a population at ≈1.46 Ma (Table 3). The isochron analysis results in omission of one older (CT8-1a) and one younger outlier (CT8-9a); the remaining 8 analyses define an isochron age of 1.479 ± 0.020 Ma, an initial $^{40}Ar/^{36}Ar$ of 250.9 ± 42.5, and a MSWD of 1.6 (Figs. 2 and 3). The mean indicates that only CT8-1a be omitted and gives an age of 1.457 ± 0.016 Ma. The weighted mean equivalent is 1.459 ± 0.008 Ma (Table 1). Once again, these age estimates all overlap at the 1σ level.

Sample CT-7 is nearly aphyric and contains dominantly plagioclase feldspar, and thus both sanidine and plagioclase were analyzed. A total of 13 fusions yielded only two sanidines; the remaining analyses were of plagioclase (identified by Ca/K > 1) (Table 3). None of these data define meaningful isochrons. The two sanidine analyses have a mean of 1.543 ± 0.066 Ma and a weighted mean of 1.520 ± 0.016 Ma, whereas the same treatment for the plagioclase analyses omits CT7-4a and yields a mean of 1.324 ± 0.016 Ma and weighted mean of 1.205 ± 0.024 Ma (Table 1). The two sanidine analyses are broadly consistent with stratigraphic relationships among other Cerro Toledo samples ages; however, the plagioclase ages are either too imprecise or too inconsistent with stratigraphic relationships to be of use in constraining ages.

Sample CT-4 is also nearly aphyric; the dominant feldspar is plagioclase, and both sanidine and plagioclase crystals were analyzed. The 6 sanidine analyses define a relatively coherent group at ca. 1.49 Ma, whereas the 10 plagioclase analyses are significantly more heterogeneous and tend to define younger ages, although there are some older ages. A sanidine isochron yields an age of 1.474 ± 0.023 Ma, an initial $^{40}Ar/^{36}Ar$ of 296.6 ± 51.4, and a MSWD of 0.4 after omitting analysis CT4-3a (Figs. 2 and 3). The 6 sanidine analyses define a mean of 1.488 ± 0.024 Ma and a weighted mean of 1.491 ± 0.009 Ma (Table 1). These ages are consistent with stratigraphic relationships. The plagioclase analyses do not define an isochron. A plagioclase mean of 1.370 ± 0.143 Ma and weighted mean of 1.287 ± 0.019 Ma include all 10 plagioclase analyses. As for CT-7, these ages are stratigraphically inconsistent or too imprecise to be useful.

Nine fusions from sample CT-3 yielded apparent ages from 1.474 to 1.998 Ma (Table 3). The isochron procedure results in omitting three of these; a resulting isochron is defined by six analyses (present as two distinct clusters) having a very narrow range of radiogenic yields (>94%, >97%), which give an age of 1.451 ± 0.022 Ma with an apparent initial $^{40}Ar/^{36}Ar$ of 714 ± 56 and a MSWD of 2.2. The mean age omits sample CT3-8a and yields 1.531 ± 0.032 Ma. The weighted mean of these data is 1.542 ± 0.008 Ma (Table 1). Because of the narrow range in radiogenic yield of the CT-3 analyses and the resulting unconstrained isochron, we take the weighted mean as the best estimate of the age of the unit (Table 1).

Sample CT-2 yielded apparent ages for 12 analyses that range from 1.200 to 1.624 Ma (Table 3). Seven of these define an isochron (omitting CT2-3a, CT2-4a, CT2-5a, CT2-12a, and CT2-13a) giving an age of 1.536 ± 0.018 Ma with an initial $^{40}Ar/^{36}Ar$ of 297.6 ± 8.1 and a MSWD of 2.2 (Figs. 2 and 3). The mean omits only CT2-12a and gives an age of 1.558 ± 0.033 Ma. The corresponding weighted mean is 1.550 ± 0.008 Ma (Table 1). These three ages are identical at the 1σ level.

We did 13 fusions on sample CT-1, which is from a pumice bed stratigraphically a few metres above the Otowi Member. These yield scattered apparent ages of 1.593 to 1.956 Ma (Table 3), with only the youngest being consistent with its stratigraphic position above the underlying Otowi Member (Fig. 4). These data fail to define an acceptable isochron regardless of how many outliers are omitted. A mean age of 1.653 ± 0.032 Ma omits CT1-7a and the corresponding weighted mean age is 1.652 ± 0.008 Ma (Table 1). Although the mean age is in agreement with the age of the Otowi Member (see below), these data add no useful constraints to the age of sample CT-1. However, its age is stratigraphically constrained to be between that of the Otowi Member and the overlying CT-2 (Table 1).

Cerro Toledo Rhyolite Domes and Otowi Member—University of Houston Data

Sanidine crystals (n = 25) from the Warm Springs dome (WS-2) exhibit the widest range in $^{40}Ar/^{39}Ar$ ages from 1.044 to 104.80 Ma (Table 3), of all samples in this study. The isochron approach excludes 10 of these analyses, most significantly older than the mode at 1.252 Ma (Fig. 3) (WS-2g–WS-2o), and one younger crystal (WS-2e), and gives an age of 1.265 ± 0.011 Ma, an atmospheric initial $^{40}Ar/^{36}Ar$ of 296 ± 15, with a MSWD of 1.1 (Fig. 2, Table 2). Analyses defining the isochron exhibit a Gaussian distribution with a mode at 1.252 Ma (Fig. 3). When including all analyses, the mean and standard deviations (6.4 ± 20.2 Ma) suggest exclusion of WS-2m only, and thus fail to identify the obvious mode of analyses at 1.252 Ma (Fig. 3). The mean and weighted mean ages of 1.267 ± 0.025 Ma and

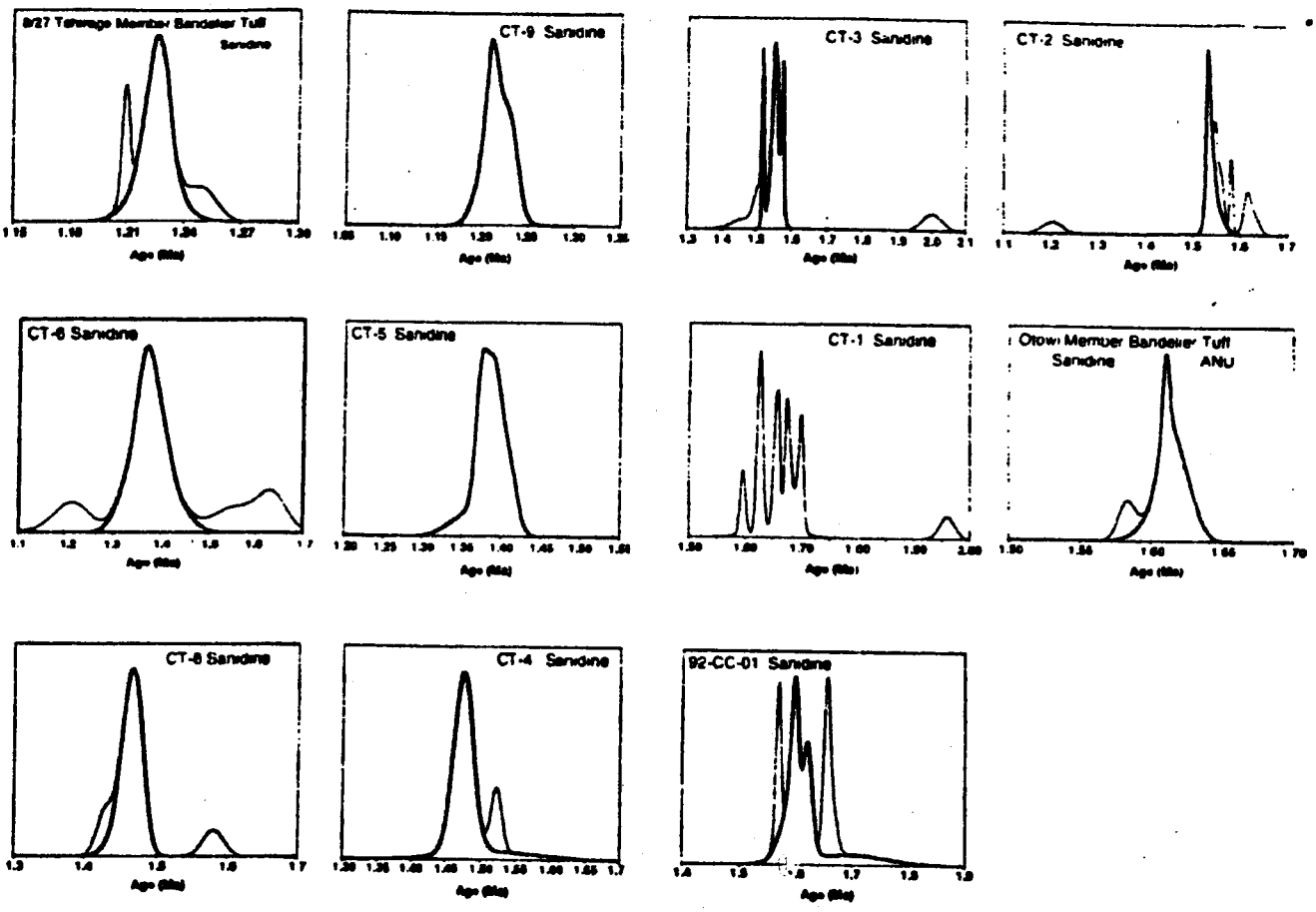

Figure 3 (Above and on facing page). Probability distribution diagrams for the data presented in Figure 2. Thicker curved lines are data used to define isochrons whereas thinner lines show all analyses from a particular unit. Note that sample 17-31 (Otowi Member) was analyzed at both the Australian National University (ANU) and the University of Houston (UofH).

1.263 ± 0.011 Ma, respectively, shown in Table 2 are calculated using the juvenile crystal population defined by the isochron approach and are indistinguishable from the isochron age.

Sample TE-9 from the Sierra de Toledo dome gave a very homogeneous population of sanidine analyses: all 10 fell on an isochron defining an age of 1.336 ± 0.018 Ma, an initial $^{40}Ar/^{36}Ar$ of 305 ± 19 and a MSWD of 0.8 (Fig. 2, Table 2). These analyses, after omitting TE-9i, give mean and weighted mean ages of 1.326 ± 0.027 Ma and 1.336 ± 0.012 Ma, respectively, which are indistinguishable from the isochron age.

Fusions of sanidine phenocrysts (n = 13) from sample TE-15 from the Turkey Ridge dome yield $^{40}Ar/^{39}Ar$ ages ranging from 1.318 to 1.927 Ma, 11 of these forming a coherent group that defines a mode at 1.343 Ma on the probability distribution plot (Fig. 3, Table 3). The isochron approach omits crystals TE-15h and TE-15j (Table 3), which have distinctly older ages than the remaining 11, and gives an age of 1.343 ± 0.015 Ma, an initial $^{40}Ar/^{36}Ar$ of 315 ± 70 and a MSWD of 1.2 (Fig. 2, Table 2). The mean and standard deviation omits analysis TE-15j (1.927 Ma), giving an age of 1.351 ± 0.026 Ma, with the corresponding weighted mean at 1.348 ± 0.021 Ma (Table 2).

Ten sanidine analyses from sample TE-1, from Unnamed dome, range in age from 1.234 Ma to 1.481 Ma, with eight clustered tightly at 1.354 Ma (Fig. 3, Table 3). The isochron approach omits TE-1d and TE-1g, which are older and younger, respectively, than the remaining analyses (Table 3). The isochron defines an age of 1.348 ± 0.010 Ma, with an initial $^{40}Ar/^{36}Ar$ of 307 ± 30 and a MSWD of 0.9 (Fig. 2). The mean and weighted means result from omission of the same analyses and are 1.356 ± 0.013 Ma and 1.357 ± 0.011 Ma, respectively.

A total of 21 sanidine fusions from sample TE-26 (Cerro Trasquilar) define a fairly homogeneous population: $^{40}Ar/^{39}Ar$ ages range from 1.224 Ma to 1.460 Ma, and 17 of these are in the range 1.321 to 1.416 Ma, giving a mode at 1.378 (Fig. 3, Table 3). The isochron (Fig. 2) is defined by these 17 analyses (TE-26f, TE-26r, and TE-26s omitted), which give an age of 1.359 ± 0.012 Ma, an initial $^{40}Ar/^{36}Ar$ of 310 ± 8 and a MSWD of 1.4 (Fig. 2, Table 2). The mean age approach omits only analysis TE-26q and gives an age of 1.368 ± 0.048 Ma with a corresponding weighted mean of 1.369 ± 0.011 Ma (Table 2).

A homogeneous population of $^{40}Ar/^{39}Ar$ ages was obtained from fusion of 21 sanidine phenocrysts from sample TE-13 (Sierra de Toledo). The isochron approach includes all analyses and gives an age of 1.379 ± 0.012 Ma, with an initial $^{40}Ar/^{36}Ar$ of 305 ± 10 and a MSWD of 0.9 (Fig. 2). The mean age omits analysis TE-13g, giving an age of 1.367 ± 0.030 Ma, and the weighted mean of these analyses is 1.380 ± 0.011 Ma (Table 2).

Sanidine fusions (n = 22) from TE-20, Los Posos East dome, gave a fairly homogeneous

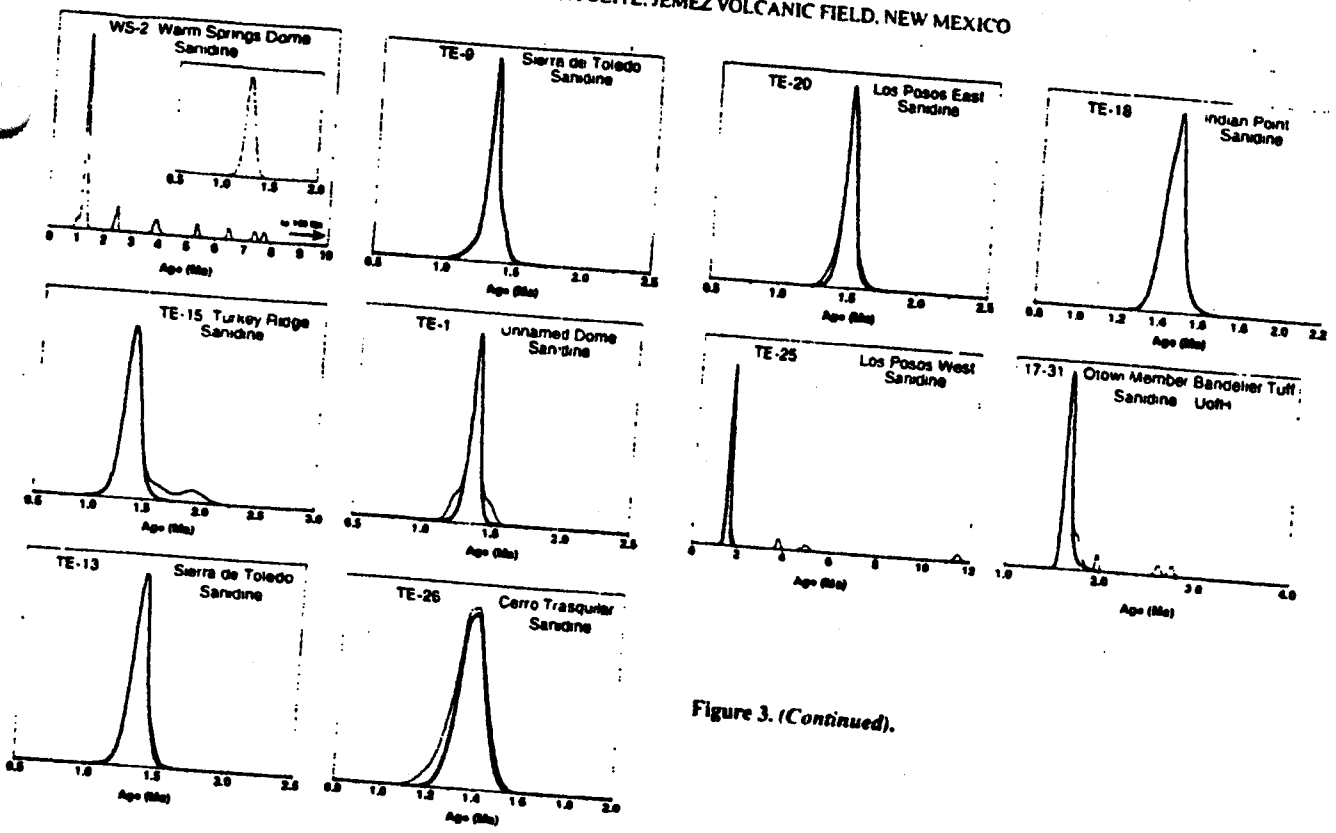

Figure 3. *(Continued).*

population defining a mode at 1.468 on the probability distribution plot (Fig. 3, Table 3). An acceptable isochron is defined after omitting TE-20r and TE-20u, giving an age of 1.446 ± 0.009 Ma, with a high initial $^{40}Ar/^{36}Ar$ of 402 ± 33, and a MSWD of 1.8 (Fig. 2). The mean age is 1.481 ± 0.027 Ma after omitting TE-20u and TE-20v, and the weighted mean age is 1.477 ± 0.009 Ma (Table 2).

Sanidine crystals (n = 25) were analyzed from sample TE-18, from the Indian Point dome (Table 3). These ages form a Gaussian distribution with a mode at 1.472 Ma (Fig. 3) and a range from 1.386 Ma to 1.533 Ma (Table 3). The isochron analysis includes all the data and gives an age of 1.463 ± 0.011 Ma, with an initial $^{40}Ar/^{36}Ar$ of 296 ± 11, and a MSWD of 1.1 (Fig. 2). The mean omits analyses TE-18c and TE-18r (older and younger than the mean, respectively) and gives an age of 1.457 ± 0.018 Ma. The corresponding weighted mean age is 1.464 ± 0.009 Ma (Table 2). All of these ages are virtually indistinguishable.

Sanidine analyses (n = 17) from sample TE-25 (Los Posos West) show a strong mode at 1.537 Ma (defined by 13 analyses) with four distinctly older outliers ranging up to 11.51 Ma (Fig. 3, Table 3). The isochron approach results in omission of these four older analyses and gives an age of 1.540 ± 0.012 Ma, with an initial $^{40}Ar/^{36}Ar$ of 302 ± 12, and a MSWD of 0.5 (Fig. 2). The mean and weighted mean ages of 1.548 ± 0.018 Ma and 1.545 ± 0.016 Ma, respectively, result from omitting the same outliers (Table 2).

Sanidine phenocrysts from sample 17-31 (Otowi Member) define $^{40}Ar/^{39}Ar$ ages ranging from 1.583 to 9.459 Ma (Table 3). Isochron analysis shows that after omitting 5 of 33 analyses (17-31[UH], 17-31l, 17-31m, 17-31s, 17-31y and 17-31af were excluded), an age of 1.618 ± 0.011 Ma is defined with a trapped $^{40}Ar/^{36}Ar$ of 301 ± 3 and a MSWD of 2.1. The 28 analyses defining the isochron form a coherent group with a mode at 1.62 Ma (Fig. 3). The corresponding mean and weighted mean ages of 1.644 ± 0.053 Ma and 1.625 ± 0.009 Ma result from omitting the same outliers as the isochron.

DISCUSSION

Bandelier Tuff

The $^{40}Ar/^{39}Ar$ ages obtained in this study of 1.225 ± 0.008 Ma (Australian National University), 1.608 ± 0.010 Ma (Australian National University) and 1.618 ± 0.011 (University of Houston) for the Tshirege Member and Otowi Member, respectively, are 9.4% older (Tshirege Member) to 11.6% older (Otowi Member) than the K-Ar dates reported by Doell et al. (1968). This difference is most likely the result of incomplete degassing of sanidine during the K-Ar analyses (e.g., Webb and McDougall, 1967; McDowell, 1983). Spell et al. (1990) obtained ages of 1.19 ± 0.02 Ma and 1.57 ± 0.03 Ma for the Tshirege Member and Otowi Member, respectively (when adjusted to an age of 27.9 Ma for the Fish Canyon Tuff; see previous discussion). Izett and Obradovich (1994) reported ages of 1.24 ± 0.02 Ma for the Tshirege Member and 1.63 ± 0.01 Ma for the Otowi Member that agree with the ages reported here and are slightly older than (although overlapping at 2σ errors) the ages reported in Spell et al. (1990).

Note that analyses of the Otowi Member sample from Cochiti Canyon (92-CC-01, from a complexly channeled outcrop) form a much more age heterogeneous group than those from sample 17-31 from the massive middle flow unit of the Otowi Member. Furthermore the much larger number of analyses of 17-31 at the University of Houston (n = 33) show the presence of xenocrysts which were not apparent from the

TABLE 3. $^{40}Ar/^{39}Ar$ ANALYTICAL DATA FOR CERRO TOLEDO RHYOLITE SAMPLES

Sample ID	^{36}Ar ($\times 10^{-18}$ mol)	^{37}Ar ($\times 10^{-17}$ mol)	^{39}Ar ($\times 10^{-15}$ mol)	^{40}Ar ($\times 10^{-15}$ mol)	$^{40}Ar^*$ (%)	Ca/K ($\times 10^{-2}$)	$^{40}Ar^*/^{39}Ar_K$	Age (Ma ± σ)
Tshirege Member Bandelier Tuff, Plinian Unit, J = 0.00039730, Australian National University								
8/27-1a	6.127	11.76	13.19	24.55	91.3	1.96	1.6997	1.218 ± 0.010
8/27-2a	5.284	8.245	9.789	18.56	90.3	1.85	1.7123	1.227 ± 0.010
8/27-3a	10.72	10.25	11.51	23.04	85.0	1.96	1.7023	1.220 ± 0.009
8/27-4a	6.789	14.12	15.14	28.22	91.6	2.05	1.7066	1.223 ± 0.008
8/27-5a	3.153	7.685	6.489	12.12	91.0	2.61	1.7047	1.221 ± 0.014
8/27-6a	10.30	12.49	13.13	25.47	86.8	2.09	1.6832	1.206 ± 0.006
8/27-7a	2.376	8.420	8.510	15.71	94.2	2.18	1.7403	1.247 ± 0.010
8/27-8a	1.230	7.502	8.396	14.92	96.2	1.97	1.7088	1.224 ± 0.008
Cerro Toledo RhyoliteTephra, Stratigraphic Level 41, ANU# 92-141, J = 0.00040904, Australian National University								
CT9-1a	2.083	6.363	6.641	11.58	93.7	2.11	1.6335	1.205 ± 0.008
CT9-2a	21.41	8.881	9.127	21.45	69.8	2.14	1.6398	1.210 ± 0.014
CT9-3a	3.164	6.682	7.128	12.86	91.8	2.06	1.6554	1.221 ± 0.012
CT9-4a	3.837	6.059	6.736	12.29	89.8	1.98	1.6380	1.208 ± 0.009
CT9-5a	2.111	4.931	5.263	9.413	92.4	2.06	1.6527	1.219 ± 0.015
CT9-6a	1.485	2.592	5.325	9.355	94.3	1.07	1.6566	1.222 ± 0.011
CT9-7a	7.783	6.269	5.220	10.96	78.2	2.64	1.6414	1.211 ± 0.016
CT9-8a	1.771	7.013	4.563	8.041	92.5	3.38	1.6305	1.203 ± 0.013
CT9-9a	1.226	6.408	5.235	8.986	95.0	2.69	1.6264	1.200 ± 0.013
CT9-10a	1.609	5.080	4.929	8.786	93.6	2.27	1.6687	1.231 ± 0.010
Cerro Toledo Rhyolite Tephra, Stratigraphic Level 38, ANU# 92-138, J = 0.00041290, Australian National University								
CT6-1a	78.31	9.212	4.890	32.56	28.7	4.14	1.9095	1.422 ± 0.034
CT6-2a	2.729	4.107	2.569	5.541	84.7	3.52	1.8264	1.360 ± 0.022
CT6-3a	1.369	3.781	1.876	3.961	89.0	4.43	1.8800	1.400 ± 0.020
CT6-5a	1.164	3.487	1.868	4.466	91.6	4.11	2.1902	1.631 ± 0.031
CT6-6a	4.145	4.880	2.114	5.124	75.4	5.08	1.8286	1.362 ± 0.021
CT6-7a	0.608	4.322	1.741	3.836	94.6	5.46	2.0840	1.552 ± 0.045
CT6-8a	15.99	2.234	0.938	6.263	24.3	5.24	1.6251	1.210 ± 0.037
CT6-9a	1.755	3.904	1.519	3.250	83.3	5.65	1.7824	1.327 ± 0.025
CT6-10a	10.29	4.116	1.350	5.544	44.8	6.71	1.8395	1.370 ± 0.021
Cerro Toledo Rhyolite Tephra, Stratigraphic Level 35, ANU# 92-137, J = 0.00041414, Australian National University								
CT5-1a	3.056	9.571	4.841	9.970	90.1	4.35	1.8567	1.387 ± 0.011
CT5-2a	1.974	11.79	7.843	15.53	95.4	3.31	1.8891	1.411 ± 0.011
CT5-3a	3.546	6.461	4.556	9.575	88.3	3.12	1.8548	1.385 ± 0.019
CT5-4a	1.398	5.509	3.740	7.414	93.6	3.24	1.8552	1.386 ± 0.015
CT5-5a	1.972	4.745	2.776	5.640	88.9	3.76	1.8056	1.349 ± 0.022
CT5-6a	2.149	6.675	3.312	6.827	89.9	4.43	1.8534	1.384 ± 0.019
CT5-7a	1.693	8.834	3.693	7.448	92.5	5.26	1.8654	1.393 ± 0.014
CT5-8a	3.363	7.030	3.113	6.845	84.8	4.97	1.8637	1.392 ± 0.011
CT5-9a	3.123	9.262	6.474	12.95	92.0	3.15	1.8406	1.375 ± 0.010
CT5-10a	2.193	9.809	4.972	9.849	92.6	4.34	1.8342	1.370 ± 0.009
Cerro Toledo Rhyolite Tephra, Stratigraphic Level 27, ANU# 92-140, J = 0.00040908, Australian National University								
CT8-1a	5.749	17.57	5.421	13.37	86.7	7.13	2.1387	1.578 ± 0.015
CT8-2a	4.824	27.01	9.395	2.034	92.3	6.33	1.9979	1.474 ± 0.010
CT8-3a	2.860	15.17	7.464	15.69	94.2	4.47	1.9802	1.461 ± 0.011
CT8-4a	2.712	13.56	7.290	15.42	94.0	4.09	1.9694	1.46[illegible] ± 0.013
CT8-5a	4.689	42.27	7.792	16.84	91.2	11.9	1.9711	1.45[illegible] ± 0.009
CT8-7a	3.674	12.77	5.084	11.15	89.5	5.52	1.9632	1.44[illegible] ± 0.017
CT8-8a	2.795	15.07	7.144	15.17	93.8	4.64	1.9919	1.46[illegible] ± 0.010
CT8-9a	2.209	9.880	4.518	9.455	92.3	4.81	1.9319	1.42[illegible] ± 0.011
CT8-10a	3.709	15.33	7.590	16.23	92.5	4.44	1.9778	1.45[illegible] ± 0.016
Cerro Toledo Rhyolite Tephra, Stratigraphic Level 22, ANU# 92-139, J = 0.00041060, Australian National University								
CT7-1a	3.487	8.208	3.320	7.786	88.1	5.44	2.0198	1.49[illegible] ± 0.018
CT7-2a	1.880	20.75	0.379	1.117	51.5	120	1.5184	1.12[illegible] ± 0.139
CT7-3a	1.658	14.49	0.250	0.911	47.4	128	1.7294	1.281 ± 0.179
CT7-4a	0.598	17.36	0.315	1.042	84.2	121	2.7912	2.06[illegible] ± 0.149
CT7-5a	1.796	21.39	0.335	1.287	60.0	141	2.3078	1.70[illegible] ± 0.103
CT7-6a	0.796	21.43	0.382	0.949	76.8	124	1.9086	1.413 ± 0.084
CT7-7a	0.572	14.73	0.291	0.745	78.6	112	2.0147	1.492 ± 0.103
CT7-8a	[illegible].839	13.07	0.261	0.738	67.6	110	1.9076	1.413 ± 0.219
CT7-9a	[illegible]57	4.995	1.497	3.666	87.6	7.34	2.1469	1.590 ± 0.027
CT7-10a	[illegible]088	17.01	0.317	1.098	44.9	118	1.5570	1.153 ± 0.059
CT7-11a	1.185	11.63	0.157	0.653	47.8	163	1.9946	1.477 ± 0.183
CT7-12a	1.318	15.48	0.251	0.714	47.1	136	1.3416	0.994 ± 0.051
CT7-13a	1.501	21.45	0.445	1.139	62.3	106	1.5941	1.180 ± 0.041
Cerro Toledo Rhyolite Tephra, Stratigraphic Level 21-22, ANU# 92-136, J = 0.00039560, Australian National University								
CT4-1a	1.178	9.250	2.918	6.465	93.6	6.98	2.0740	1.480 ± 0.013
CT4-2a	1.688	31.42	0.623	1.634	70.5	111	1.6881	1.320 ± 0.045
CT4-3a	1.549	16.73	3.645	8.306	93.6	10.1	2.1321	1.521 ± 0.011
CT4-4a	0.796	17.15	0.347	0.975	76.8	109	2.1564	1.538 ± 0.150
CT4-5a	1.166	30.49	0.615	1.691	80.5	109	2.2148	1.580 ± 0.070
CT4-6a	1.202	6.726	3.002	6.644	93.6	4.93	2.0712	1.478 ± 0.017

(Continued)

TABLE 3. *(Continued)*

Sample ID	^{36}Ar (× 10^{-18} mol)	^{37}Ar (× 10^{-17} mol)	^{39}Ar (× 10^{-15} mol)	^{40}Ar (× 10^{-15} mol)	$^{40}Ar^*$ (%)	Ca/K (× 10^{-2})	$^{40}Ar^*/^{39}Ar_K$	Age (Ma ± σ)
Cerro Toledo Rhyolite Tephra, Stratigraphic Level 21-22, ANU# 92-136, J = 0.00039560, Australian National University *(continued)*								
CT4-7a	1.972	33.33	0.633	1.566	64.0	116	1.5841	1.130 ± 0.028
CT4-8a	1.563	6.050	2.309	5.260	90.2	5.76	2.0550	1.466 ± 0.014
CT4-9a	1.459	11.69	3.555	7.836	93.5	7.24	2.0609	1.470 ± 0.017
CT4-10a	9.040	25.21	0.474	1.259	79.9	1.17	2.1234	1.515 ± 0.073
CT4-11a	1.452	27.66	0.521	1.435	71.1	117	1.9590	1.398 ± 0.036
CT4-12a	1.820	33.69	0.584	1.599	67.6	127	1.8525	1.322 ± 0.076
CT4-13a	1.728	15.35	0.305	1.014	50.4	111	1.6762	1.196 ± 0.177
CT4-14a	1.377	17.75	0.3761	1.089	63.4	104	1.8364	1.310 ± 0.093
CT4-16a	1.273	15.26	0.288	0.962	61.8	116	2.0619	1.471 ± 0.143
CT4-19a	1.333	18.85	0.256	0.895	57.4	162	2.0091	1.433 ± 0.167
Cerro Toledo Rhyolite Tephra, Stratigraphic Level 18, J = 0.00039400, Australian National University								
CT3-1a	5.132	42.94	23.72	52.58	96.0	3.98	2.1293	1.513 ± 0.008
CT3-2a	2.212	8.713	5.487	12.72	93.8	3.49	2.1741	1.545 ± 0.011
CT3-3a	6.530	26.14	17.12	40.14	94.2	3.36	2.2080	1.569 ± 0.009
CT3-4a	0.807	9.970	6.327	14.09	97.2	3.47	2.1656	1.539 ± 0.015
CT3-5a	2.321	10.68	5.873	13.62	93.9	4.00	2.1791	1.548 ± 0.010
CT3-6a	2.559	7.209	3.304	7.823	89.3	4.80	2.1157	1.503 ± 0.015
CT3-7a	131.4	14.04	4.947	49.20	20.9	6.24	2.0739	1.474 ± 0.044
CT3-8a	2.495	52.45	0.521	2.181	67.8	2.22	2.8120	1.998 ± 0.030
CT3-9a	1.192	7.179	3.525	8.175	94.7	4.48	2.1959	1.560 ± 0.013
Cerro Toledo Rhyolite Tephra, Stratigraphic Level 14, J = 0.00039370, Australian National University								
CT2-1a	10.44	34.53	12.19	29.79	88.7	6.23	2.1686	1.540 ± 0.013
CT2-2a	3.642	22.02	8.162	18.83	93.3	5.94	2.1522	1.528 ± 0.008
CT2-3a	8.763	39.49	11.27	27.89	89.8	7.71	2.2239	1.579 ± 0.008
CT2-4a	2.557	20.87	7.135	17.24	94.7	6.43	2.2879	1.624 ± 0.014
CT2-5a	6.976	40.06	13.77	32.58	92.7	6.40	2.1932	1.557 ± 0.010
CT2-6a	2.951	41.92	10.63	24.33	95.5	8.67	2.1851	1.551 ± 0.017
CT2-7a	2.099	16.07	8.223	18.52	95.6	4.30	2.1529	1.529 ± 0.010
CT2-8a	21.32	19.01	8.077	23.98	72.9	5.18	2.1656	1.538 ± 0.010
CT2-9a	3.729	26.07	12.41	28.14	95.0	4.62	2.1543	1.530 ± 0.009
CT2-10a	5.626	39.51	8.607	21.37	91.4	10.1	2.2689	1.611 ± 0.011
CT2-11a	3.127	19.69	7.528	17.49	93.7	5.76	2.1773	1.546 ± 0.009
CT2-12a	1.644	5.401	2.601	4.943	88.9	4.57	1.6898	1.200 ± 0.022
Cerro Toledo Rhyolite Tephra, Stratigraphic Level 8, J = 0.00039581, Australian National University								
CT1-1a	9.599	36.90	20.36	50.58	93.4	3.99	2.3214	1.657 ± 0.009
CT1-2a	5.633	23.49	11.98	30.11	93.5	4.31	2.3501	1.677 ± 0.010
CT1-3a	4.576	27.93	13.53	33.86	95.1	4.54	2.3802	1.699 ± 0.009
CT1-4a	2.732	27.19	17.80	41.81	97.0	3.36	2.2794	1.627 ± 0.009
CT1-5a	3.703	32.37	18.39	44.60	96.6	3.87	2.3416	1.671 ± 0.009
CT1-6a	8.282	22.61	10.74	28.18	90.4	4.63	2.3724	1.695 ± 0.010
CT1-7a	163.3	30.97	14.16	87.39	44.4	4.81	2.7407	1.956 ± 0.017
CT1-8a	2.193	2.326	0.818	2.559	74.0	6.26	2.3147	1.652 ± 0.050
CT1-9a	24.41	14.28	9.457	28.93	74.3	3.32	2.2721	1.622 ± 0.009
CT1-10a	5.968	14.88	8.447	21.51	90.9	3.88	2.3135	1.651 ± 0.009
CT1-11a	3.806	16.04	11.15	26.73	94.8	3.17	2.2728	1.622 ± 0.009
CT1-12a	3.048	14.19	8.222	19.45	94.4	3.80	2.2322	1.593 ± 0.009
CT1-13a	145.7	23.03	11.03	69.04	37.2	4.60	2.3322	1.665 ± 0.019
Otowi Member Bandelier Tuff, Middle Flow Unit, J = 0.00040092, Australian National University								
17-31-1a	24.31	21.37	12.35	34.90	78.6	3.81	2.2199	1.605 ± 0.009
17-31-2a	14.28	20.64	10.46	27.80	83.9	4.34	2.2319	1.614 ± 0.009
17-31-3a	11.91	31.68	20.61	81.96	56.4	3.38	2.2447	1.623 ± 0.012
17-31-4a	16.57	50.30	24.58	60.15	90.9	4.50	2.2238	1.608 ± 0.008
17-31-5a	2.094	12.36	6.305	14.54	94.7	4.31	2.1850	1.580 ± 0.010
17-31-6a	7.556	13.32	7.099	18.31	86.9	4.13	2.2409	1.620 ± 0.011
17-31-7a	39.35	13.22	7.011	27.33	56.8	4.15	2.2157	1.602 ± 0.016
17-31-8a	84.97	29.75	17.62	64.62	60.5	3.72	2.2184	1.604 ± 0.012
Otowi Member Bandelier Tuff, Cochiti Canyon, J = 0.00039975, Australian National University								
92CC1-1a	248.3	8.636	5.385	86.14	14.7	3.53	2.3448	1.690 ± 0.067
92CC1-2a	28.62	19.68	12.61	37.06	76.4	3.44	2.2449	1.618 ± 0.011
92CC1-3a	5.152	18.94	10.19	25.19	93.0	4.09	2.2449	1.658 ± 0.013
92CC1-4a	152.5	15.98	10.24	67.95	33.3	3.43	2.2095	1.593 ± 0.018
92CC1-5a	3.877	12.06	5.685	13.63	90.6	4.67	2.1723	1.566 ± 0.009
92CC1-6a	1.629	4.197	2.022	4.987	89.4	4.57	2.2052	1.590 ± 0.024
92CC1-7a	2.104	9.520	5.478	12.87	94.2	3.82	2.2119	1.594 ± 0.010
92CC1-8a	5.298	14.62	12.22	29.85	93.8	2.63	2.2905	1.651 ± 0.010
Cerro Toledo Rhyolite, Warm Springs Dome, J = 0.000561, University of Houston								
WS-2a	0.784	5.238	4.957	6.397	96.5	1.91	1.2478	1.262 ± 0.032
WS-2b	1.568	4.844	5.364	6.972	93.5	1.63	1.2175	1.232 ± 0.026
WS-2c	2.464	5.215	5.079	6.893	89.6	1.86	1.2191	1.233 ± 0.032
WS-2d	3.248	1.857	2.212	3.673	74.1	1.52	1.2337	1.248 ± 0.059

(Continued)

TABLE 3 *(Continued)*

Sample ID	^{36}Ar (× 10^{-18} mol)	^{37}Ar (× 10^{-17} mol)	^{39}Ar (× 10^{-15} mol)	^{40}Ar (× 10^{-15} mol)	$^{40}Ar^*$ (%)	Ca/K (× 10^{-2})	$^{40}Ar^*/^{39}Ar_K$	Age (Ma ± σ)
Cerro Toledo Rhyolite, Warm Springs Dome, J = 0.000561, University of Houston *(continued)*								
WS-2e	2 752	2 924	2 852	3 730	78.6	1.86	1.0320	1 044 ± 0 063
WS-2f	1 696	1 777	1 940	2 883	82 9	1.66	1.2369	1.251 ± 0 083
WS-2g	3 536	1 757	2 832	7 996	87.2	1 12	2 4727	2 501 ± 0 0[illegible]
WS-2h	77 088	2 089	2 413	31 682	29.5	1.57	3 8930	3 936 ± 0.089
WS-2i	17.280	1 636	1 618	17.344	71.2	1 83	7 6633	7 739 ± 0.076
WS-2j	1 216	0 994	1.251	8.337	95 8	1 44	6 4118	6.478 ± 0 063
WS-2k	6 352	2.033	2.029	6.660	72 4	1 81	2.3879	2 415 ± 0 046
WS-2l	13 152	2 314	2 232	15 628	75.6	1.88	5 3190	5 375 ± 0 053
WS-2m	54 032	1 340	0 883	109 376	85 7	2.75	106 6100	104 795 ± 0 625
WS-2n	3 440	1 246	1 307	10 516	90.5	1.73	7 3156	7 389 ± 0 077
WS-2o	1 232	1 076	0.883	3 738	90 4	2.21	3.8324	3.874 ± 0 082
WS-2p	2 096	0 588	1 387	2 283	73.3	0 78	1 2274	1.242 ± 0 054
WS-2q	0.976	0.239	1 044	1 582	82.0	0 42	1 2457	1.260 ± 0 072
WS-2r	0 080	1 512	2 458	3 199	99 4	1 11	1.2960	1 311 ± 0.031
WS-2s	1 120	1.808	3.104	4 192	92.2	1 05	1 2480	1.263 ± 0.028
WS-2t	3 232	2 228	1 278	2 534	62.8	3 16	1 2489	1 264 ± 0.057
WS-2u	0 640	0 000	2 800	3 791	95 1	0 00	1 2904	1 305 ± 0 030
WS-2v	1 952	4 902	1 390	2 333	75 8	6 38	1.2748	1 290 ± 0 057
WS-2w	1 824	3 940	2 924	4 177	87.3	2 44	1 2501	1 265 ± 0 027
WS-2x	0 304	1 006	1 228	1 663	94 7	1 48	1 2842	1.299 ± 0 061
WS-2y	0 480	3 959	1 230	1 702	91 9	5 83	1 2745	1 289 ± 0 055
WS-2z	0 160	4 419	2 410	3 015	98 6	3 32	1 2357	1.250 ± 0 030
Cerro Toledo Rhyolite, Sierra de Toledo, J = 0.000558, University of Houston								
TE-9a	5 088	12 455	8 899	13 310	88 9	2 53	1 3326	1 341 ± 0 018
TE-9b	6 976	8 661	5 425	9 220	77 9	2 89	1 3274	1 336 ± 0 027
TE-9c	2 112	6.876	4 809	6 968	91.2	2 59	1 3248	1 333 ± 0 031
TE-9d	3 312	6 673	4 722	7 149	86.5	2 56	1 3127	1 321 ± 0 032
TE-9e	2 592	4.666	3 028	4 769	84 3	2 79	1.3328	1 341 ± 0.049
TE-9f	8 816	3.061	2 349	5 652	54 7	2 36	1 3226	1 331 ± 0 068
TE-9g	1 760	2.839	1 454	2 419	79.1	3.53	1 3211	1 329 ± 0.111
TE-9h	0 368	1.859	1 606	2 254	95 3	2 10	1 3431	1 351 ± 0 037
TE-9i	1 392	1 158	0 821	1 425	71 7	2 55	1 2504	1 258 ± 0 090
TE-9j	1 984	2.293	1 678	2 936	80 6	2 47	1 4163	1 425 ± 0 037
Cerro Toledo Rhyolite, Turkey Ridge, J = 0.000554, University of Houston								
TE-15a	0 208	3 091	2 403	3 311	98.2	2.33	1 3559	1 355 ± 0 060
TE-15b	0 160	0.867	1 078	1 472	97 0	1 46	1 3277	1 326 ± 0 147
TE-15c	0 288	2.813	1.682	2 339	96 5	3.03	1 3450	1 344 ± 0 112
TE-15d	0 208	3.852	2 564	3 433	98 3	2.72	1 3196	1 318 ± 0.061
TE-15e	0 624	1 820	1 497	2 147	91 7	2.20	1 3200	1 319 ± 0 043
TE-15f	0 992	1 969	1 178	1 861	84 6	3 03	1 3418	1.341 ± 0 061
TE-15g	0 160	1 654	1 222	1 734	97 4	2 45	1 3885	1.387 ± 0.057
TE-15h	4 848	1.302	0 854	2 787	49 3	2 76	1.6122	1 611 ± 0.096
TE-15i	0 752	3.029	0 886	1 447	84.9	6 14	1 3897	1.388 ± 0 087
TE-15j	0 128	0 424	0 839	1 650	97 8	0 90	1 9288	1 927 ± 0 101
TE-15k	1 104	0 000	1 400	2 217	85 4	0 00	1 3562	1 355 ± 0.070
TE-15l	0 096	3.314	1 003	1 413	98.2	5 91	1 3869	1.386 ± 0 075
TE-15m	0.064	3.647	1 084	1 473	98 9	6 02	1 3473	1 346 ± 0.072
Cerro Toledo Rhyolite, Unnamed Dome, J = 0.0005515, University of Houston								
TE-1a	1 568	6 273	4 028	5.984	92 4	2 80	1 3753	1.368 ± 0 038
TE-1b	2.896	6.616	3 643	5 772	85 4	3 05	1.3558	1 348 ± 0.042
TE-1c	1 952	6.334	3 979	6.032	90 6	2 87	1.3766	1 369 ± 0 036
TE-1d	0 704	5 175	3 008	4 688	95 7	3 10	1 4891	1 481 ± 0.043*
TE-1e	2 176	2.606	3 730	5 710	88 9	3.08	1 3640	1.357 ± 0.045
TE-1f	4 432	5.147	3 098	5.519	76 8	2.97	1 3747	1 367 ± 0.027
TE-1g	1 664	4 115	1 807	2 709	82 4	4 09	1 2402	1.234 ± 0 039*
TE-1h	0 416	3.723	0 999	1 463	91 9	6 71	1.3491	1 342 ± 0 073
TE-1i	3 744	8.321	4 689	7 447	85 4	3 19	1 3593	1.352 ± 0 018
TE-1j	0 160	7.643	1 502	2 065	98 0	9 11	1 3503	1.343 ± 0.048
Cerro Toledo Rhyolite, Cerro Trasquilar, J = 0.0005356, University of Houston								
TE-26a	1 664	3 951	2 739	4 291	88 7	2 60	1 3926	1 345 ± 0 053
TE-26b	1 616	4.472	3 514	5 309	91 2	2.29	1.3806	1.333 ± 0.037
TE-26c	0 576	2 773	2 213	3.245	95.0	2.26	1.3952	1 347 ± 0.065
TE-26d	3.504	12.514	8 637	12 992	92.2	2 61	1 3900	1 342 ± 0 020
TE-26e	1 248	2 842	2.338	3 70[illegible]	90.2	2 19	1 4337	1 384 ± 0.058
TE-26f	0 304	1 789	1 378	2 16[illegible]	96.0	2.33	1.5122	1 460 ± 0 050*
TE-26g	1 920	2.244	1 626	2 92[illegible]	81 0	2 47	1 4659	1 416 ± 0 040
TE-26h	0 336	1.663	1 272	1 903	95 0	2 34	1 4276	1.379 ± 0 043
TE-26i	1 024	2.162	1 756	2 843	89.6	2.21	1.4565	1 406 ± 0 034
TE-26j	0 736	1.685	1.212	1 924	89.0	2.49	1 4183	1.370 ± 0 059
TE-26k	4 448	6 001	3.944	6 949	81 4	2 74	1 4380	1.389 ± 0 019
TE-26l	1 082	3.845	1 764	5 747	45.2	3.92	1 4773	1 427 ± 0 047
TE-26m	6 000	2.897	1 622	4 007	56 4	3 20	1.3960	1.348 ± 0 049
TE-26n	0 320	2 372	0 770	1 180	92 3	5 53	1 4171	1 359 ± 0 073

(Continued)

TABLE 3 *(Continued)*

Sample ID	^{36}Ar (× 10^{-18} mol)	^{37}Ar (× 10^{-17} mol)	^{39}Ar (× 10^{-15} mol)	^{40}Ar (× 10^{-15} mol)	$^{40}Ar^*$ (%)	Ca/K (× 10^{-2})	$^{40}Ar^*/^{39}Ar_K$	Age (Ma ± σ)
Cerro Toledo Rhyolite, Cerro Trasquilar, J = 0.0005355, University of Houston *(continued)*								
TE-26o	0.864	2.294	1.961	2.996	91.7	2.09	1.4039	1.356 ± 0.028
TE-26p	0.688	2.373	1.022	1.594	87.5	4.16	1.3682	1.321 ± 0.049
TE-26q	1.232	1.847	1.101	1.750	79.6	3.00	1.2672	1.224 ± 0.055
TE-26r	1.088	1.558	0.990	1.616	80.5	2.85	1.3165	1.271 ± 0.069*
TE-26s	1.232	0.000	2.037	3.067	88.3	0.00	1.3324	1.287 ± 0.037*
TE-26t	2.672	0.359	1.849	3.523	78.0	0.36	1.4884	1.437 ± 0.040
TE-26u	0.896	0.001	1.366	2.197	88.1	0.00	1.4202	1.372 ± 0.049
Cerro Toledo Rhyolite, Sierra de Toledo, J = 0.0005475, University of Houston								
TE-13a	2.032	4.197	2.967	4.524	86.9	2.55	1.3279	1.311 ± 0.044
TE-13b	0.432	4.203	3.105	4.612	97.3	2.43	1.4480	1.430 ± 0.052
TE-13c	0.576	2.122	1.417	2.083	92.1	2.69	1.3569	1.340 ± 0.113
TE-13d	4.880	9.687	6.456	10.305	86.2	2.70	1.3793	1.362 ± 0.027
TE-13e	0.832	2.939	2.189	3.185	92.5	2.41	1.3492	1.332 ± 0.069
TE-13f	0.416	2.011	2.162	3.129	96.2	1.67	1.3983	1.381 ± 0.038
TE-13g	1.680	2.812	1.983	3.434	85.9	2.54	1.4940	1.475 ± 0.038
TE-13h	9.408	4.422	2.822	6.716	59.4	2.80	1.4209	1.403 ± 0.031
TE-13i	0.192	1.211	0.930	1.369	96.1	2.33	1.4219	1.404 ± 0.070
TE-13j	0.400	1.364	0.866	1.291	91.1	2.81	1.3628	1.346 ± 0.072
TE-13k	0.848	1.728	1.808	2.697	90.9	1.72	1.3595	1.342 ± 0.036
TE-13l	1.504	2.021	2.108	3.369	87.0	1.72	1.3940	1.376 ± 0.031
TE-13m	0.352	1.278	1.442	2.092	95.2	1.58	1.3844	1.367 ± 0.046
TE-13n	0.976	5.758	3.785	5.630	95.0	2.74	1.4239	1.406 ± 0.018
TE-13o	0.528	1.173	1.255	1.869	91.9	1.67	1.3716	1.354 ± 0.054
TE-13p	0.336	1.334	1.250	1.840	94.8	1.91	1.3979	1.380 ± 0.052
TE-13q	0.560	1.209	3.673	5.344	97.0	0.59	1.4141	1.396 ± 0.023
TE-13r	0.992	2.097	1.123	1.820	84.2	3.34	1.3682	1.351 ± 0.085
TE-13s	0.688	2.744	2.139	3.115	93.6	2.29	1.3658	1.349 ± 0.039
TE-13t	0.240	0.001	0.754	1.116	93.8	0.00	1.3904	1.373 ± 0.089
TE-13u	0.960	2.302	1.266	1.982	86.0	3.29	1.3491	1.332 ± 0.066
Cerro Toledo Rhyolite, Los Posos East, J = 0.000544, University of Houston								
TE-20a	0.224	6.412	3.671	5.672	98.9	3.15	1.5321	1.503 ± 0.049
TE-20b	0.048	6.678	4.973	7.350	99.9	2.42	1.4792	1.451 ± 0.030
TE-20c	0.016	5.346	3.469	5.048	100.0	2.78	1.4584	1.431 ± 0.048
TE-20d	0.320	20.510	14.603	21.812	99.7	2.53	1.4917	1.463 ± 0.012
TE-20e	0.416	3.322	2.445	3.696	96.8	2.45	1.4667	1.439 ± 0.061
TE-20f	1.264	2.317	1.915	3.299	88.8	2.18	1.5334	1.504 ± 0.084
TE-20g	0.352	2.456	2.079	3.148	96.8	2.12	1.4719	1.444 ± 0.034
TE-20h	2.528	4.478	3.053	5.400	86.5	2.63	1.5366	1.507 ± 0.029
TE-20i	0.304	1.944	1.636	2.575	96.6	2.13	1.5249	1.496 ± 0.049
TE-20j	0.016	2.807	1.942	2.954	99.9	2.59	1.5266	1.498 ± 0.037
TE-20k	2.848	5.050	3.215	5.603	85.3	2.81	1.4938	1.465 ± 0.030
TE-20l	0.160	1.776	1.197	1.826	97.5	2.67	1.4912	1.463 ± 0.050
TE-20m	1.840	1.354	0.752	1.701	68.5	3.25	1.5520	1.522 ± 0.082
TE-20n	0.320	5.627	2.829	4.321	97.9	3.58	1.4992	1.471 ± 0.022
TE-20o	0.480	4.438	2.289	3.559	96.2	3.47	1.4986	1.470 ± 0.032
TE-20p	1.200	5.432	2.909	4.767	92.7	3.31	1.5227	1.494 ± 0.024
TE-20q	0.976	10.799	4.515	7.110	96.1	4.30	1.5172	1.488 ± 0.018
TE-20r	0.128	12.329	3.741	5.809	99.5	5.92	1.5487	1.519 ± 0.022*
TE-20s	0.160	7.433	2.031	3.090	98.7	6.57	1.5045	1.476 ± 0.036
TE-20t	0.224	8.199	1.498	2.357	97.5	9.83	1.5370	1.508 ± 0.048
TE-20u	0.656	1.850	1.908	2.840	93.3	1.75	1.3917	1.365 ± 0.040*
TE-20v	1.200	1.529	1.801	3.243	89.2	1.53	1.6106	1.580 ± 0.038
Cerro Toledo Rhyolite, Indian Point, J = 0.0005395, University of Houston								
TE-18a	3.104	8.545	5.446	9.308	90.3	2.82	1.5464	1.504 ± 0.028
TE-18b	2.976	8.676	5.487	9.054	90.5	2.85	1.4958	1.455 ± 0.033
TE-18c	1.056	4.228	3.423	5.687	94.7	2.22	1.5759	1.533 ± 0.048
TE-18d	1.328	2.19*	1.663	2.958	86.9	2.37	1.5484	1.506 ± 0.080
TE-18e	8.304	14.512	10.768	18.695	87.1	2.43	1.5149	1.474 ± 0.015
TE-18f	1.696	14.369	8.530	13.456	96.4	3.03	1.5240	1.483 ± 0.017
TE-18g	5.488	7.756	4.941	9.052	82.3	2.83	1.5106	1.470 ± 0.029
TE-18h	0.928	2.242	1.742	2.782	90.4	2.31	1.4507	1.411 ± 0.038
TE-18i	0.240	2.242	1.143	1.759	96.1	3.51	1.4860	1.446 ± 0.062
TE-18j	0.832	4.423	2.635	4.106	94.3	3.00	1.4754	1.435 ± 0.030
TE-18k	0.480	3.572	2.272	3.525	96.2	2.81	1.4984	1.458 ± 0.030
TE-18l	4.432	4.029	2.687	5.323	76.0	2.68	1.5118	1.471 ± 0.027
TE-18m	0.288	3.235	1.737	2.673	97.0	3.33	1.4992	1.459 ± 0.043
TE-18n	0.608	4.068	3.167	4.835	96.4	2.30	1.4756	1.436 ± 0.025
TE-18o	0.512	1.057	1.227	1.957	92.3	1.55	1.4766	1.436 ± 0.057
TE-18p	2.032	2.855	2.116	3.646	83.9	2.43	1.4487	1.409 ± 0.033
TE-18q	0.656	1.084	1.567	2.568	92.7	1.23	1.5217	1.480 ± 0.046
TE-18r	1.728	3.043	1.939	3.258	84.6	2.82	1.4251	1.386 ± 0.040
TE-18s	0.544	3.149	2.387	3.617	95.7	2.36	1.4535	1.414 ± 0.029
TE-18t	2.016	2.674	1.707	3.081	81.1	2.82	1.4666	1.427 ± 0.046
TE-18u	0.944	2.879	2.246	3.638	92.5	2.31	1.5012	1.461 ± 0.040
TE-18v	7.680	1.081	2.560	6.024	62.8	0.76	1.4821	1.442 ± 0.036

(Continued)

TABLE 3. *(Continued)*

Sample ID	^{36}Ar (× 10^{-18} mol)	^{37}Ar (× 10^{-17} mol)	^{39}Ar (× 10^{-15} mol)	^{40}Ar (× 10^{-15} mol)	$^{40}Ar^*$ (%)	Ca/K (× 10^{-2})	$^{40}Ar^*/^{39}Ar_K$	Age (Ma ± σ)
Cerro Toledo Rhyolite, Indian Point. J = 0.0005396, University of Houston *(continued)*								
TE-18w	5.488	6.485	2.076	6.198	74.3	3.79	1.5002	1.459 ± 0.030
TE-18x	0.496	2.886	1.814	2.911	95.1	2.86	1.5290	1.488 ± 0.045
TE-18y	0.720	2.204	3.038	4.856	95.7	1.29	1.5333	1.492 ± 0.020
Cerro Toledo Rhyolite, Los Posos West. J = 0.000565, University of Houston								
TE-25a	0.800	4.784	1.814	3.020	92.3	4.75	1.5404	1.569 ± 0.076
TE-25b	0.672	10.086	2.667	4.224	85.5	6.80	1.5161	1.545 ± 0.055
TE-25c	4.320	12.626	7.098	11.892	89.5	3.20	1.5060	1.534 ± 0.021
TE-25d	1.744	4.427	2.546	4.457	88.7	3.12	1.5575	1.587 ± 0.048
TE-25e	0.448	2.639	1.264	2.048	93.9	3.75	1.5277	1.556 ± 0.096
TE-25f	1.068	3.359	0.896	1.653	81.2	6.70	1.5028	1.531 ± 0.068
TE-25g	1.232	2.483	1.390	2.463	85.6	3.19	1.5231	1.552 ± 0.048
TE-25h	0.448	2.094	0.993	1.631	92.3	3.77	1.5219	1.551 ± 0.066
TE-25i	0.448	2.841	1.646	2.618	95.1	3.09	1.5188	1.547 ± 0.042
TE-25j	0.720	1.401	0.903	1.575	87.0	2.78	1.5226	1.551 ± 0.063
TE-25k	2.784	2.474	0.693	8.644	90.6	6.39	11.3239	11.506 ± 0.131*
TE-25l	0.320	2.200	0.906	1.432	93.6	4.39	1.4821	1.510 ± 0.077
TE-25m	1.008	1.958	0.848	3.458	91.6	4.12	3.7438	3.812 ± 0.082*
TE-25n	0.304	1.347	0.477	2.407	96.4	5.07	4.8759	4.963 ± 0.155*
TE-25o	0.768	0.000	0.933	1.812	87.5	0.00	1.7036	1.736 ± 0.085*
TE-25p	2.688	3.059	0.779	1.961	60.2	7.06	1.5192	1.548 ± 0.102
TE-25q	0.400	2.599	0.963	1.565	92.6	4.85	1.508	1.537 ± 0.082
Otowi Member Bandelier Tuff, Middle Flow Unit. J = 0.0005670, University of Houston								
1731UH-1a	10.416	14.603	8.232	16.258	81.3	3.20	1.6098	1.646 ± 0.026
1731UH-1b	5.568	9.922	5.848	10.988	85.2	3.06	1.6053	1.641 ± 0.031
1731UH-1c	4.800	6.080	3.907	8.047	82.6	2.80	1.7057	1.744 ± 0.051
1731UH-1d	11.522	7.566	5.076	11.553	70.8	2.68	1.6150	1.651 ± 0.038
1731UH-1e	9.600	8.788	5.690	11.865	76.4	2.78	1.5967	1.623 ± 0.029
1731UH-1f	21.984	15.999	7.554	18.298	64.9	3.81	1.5758	1.611 ± 0.027
1731UH-1g	15.280	8.445	5.327	12.754	65.1	2.85	1.5615	1.597 ± 0.035
1731UH-1h	31.344	19.553	11.837	27.835	67.4	2.96	1.5901	1.626 ± 0.022
1731UH-1i	6.784	22.873	13.135	22.394	91.3	3.12	1.5626	1.598 ± 0.014
1731UH-1j	72.480	14.249	9.641	36.428	42.2	2.65	1.6025	1.638 ± 0.032
1731UH-1k	3.776	11.176	6.635	11.516	90.6	3.02	1.5783	1.614 ± 0.022
1731UH-1l	17.728	7.274	4.457	16.472	68.9	2.93	2.5564	2.613 ± 0.031*
1731UH-1m	15.552	4.878	3.619	37.699	88.1	2.41	9.2714	9.459 ± 0.060*
1731UH-1n	11.920	5.286	2.971	8.542	59.6	3.18	1.7217	1.760 ± 0.037
1731UH-1o	1.760	7.653	4.100	6.967	92.7	3.35	1.5636	1.619 ± 0.024
1731UH-1p	3.264	5.697	3.434	6.470	85.3	3.06	1.6116	1.648 ± 0.025
1731UH-1q	1.360	4.901	3.076	5.236	92.5	2.86	1.5780	1.614 ± 0.023
1731UH-1r	2.832	3.659	2.507	5.213	84.2	2.77	1.7544	1.794 ± 0.072
1731UH-1s	0.080	3.960	3.045	8.199	99.8	2.34	2.6934	2.753 ± 0.029*
1731UH-1t	2.400	4.969	3.994	7.116	90.3	3.58	1.6125	1.649 ± 0.019
1731UH-1u	0.592	7.872	4.673	7.634	97.9	3.03	1.6023	1.638 ± 0.019
1731UH-1v	1.712	4.464	2.338	4.131	88.0	3.42	1.5578	1.593 ± 0.036
1731UH-1w	45.136	4.806	3.265	18.441	28.7	2.64	1.6221	1.658 ± 0.045
1731UH-1x	2.016	5.622	2.892	5.094	88.5	2.83	1.5630	1.598 ± 0.025
1731UH-1y	5.904	6.519	4.321	10.010	82.8	2.70	1.9238	1.967 ± 0.020*
1731UH-1z	3.968	5.507	3.009	5.891	80.5	3.30	1.5786	1.614 ± 0.019
1731UH-1aa	0.944	0.860	1.447	2.691	89.9	1.08	1.6744	1.712 ± 0.042
1731UH-1ab	3.024	5.440	2.636	5.263	83.3	3.46	1.5496	1.584 ± 0.022
1731UH-1ac	3.168	1.608	1.989	4.176	77.9	1.46	1.6386	1.675 ± 0.029
1731UH-1ad	0.816	5.290	3.180	5.253	96.6	2.98	1.5820	1.617 ± 0.018
1731UH-1ae	2.624	4.392	1.758	3.477	78.1	4.50	1.5478	1.583 ± 0.030
1731UH-1af	1.120	0.902	1.945	3.659	91.1	0.83	1.7169	1.755 ± 0.031*
1731UH-1ag	0.128	4.005	1.312	2.184	98.4	5.50	1.6419	1.679 ± 0.044

Note: Errors on ages quoted at 1σ and include 0.5% error in J. *Samples omitted from isochron analysis.

smaller analytical set at the Australian National University (n = 8). These differences serve to illustrate the potential for variability introduced both by the sample and by the number of analyses in the analyzed crystal population.

Cerro Toledo Rhyolite Tephra

The $^{40}Ar/^{39}Ar$ ages obtained in this study are broadly consistent with previously reported K-Ar and fission-track data (Doell et al., 1968; Izett et al., 1981; Stix et al., 1988; Tables 1 and 2). Cerro Toledo Rhyolite tephra sample CT-9, dated here as 1.212 ± 0.009 Ma, may correspond to the upper pumice unit dated by Izett et al. (1981) as 1.23 ± 0.02 Ma. Although CT-9 is stratigraphically below the Tshirege Member Plinian unit, the two ages are indistinguishable within analytical errors. This indicates that significant eruptive activity was occurring within the Cerro Toledo Rhyolite prior to eruption of the Tshirege Member and collapse of the Valles caldera. Sample CT-8 has a $^{40}Ar/^{39}Ar$ age of 1.479 ± 0.020 Ma and compares favorably with a K-Ar age of 1.52 ± 0.04 Ma reported by Stix et al. (1988) on a sample from the same stratigraphic level. Although our sample CT-7 gave no reliable date, it correlates stratigraphically with CT-4 (1.474 Ma) and the lower pumice unit of Izett et al. (1981) dated as 1.47 ± 0.04 Ma by K-Ar (Table 1).

The new $^{40}Ar/^{39}Ar$ ages are shown in Figure 4 in relation to their stratigraphic position. There is agreement between the ages, including those of the bracketing Bandelier tuffs, and stratigraphic level in the tephra sequence. Overall, the samples fall into groups with ages of ca. 1.54, 1.48,

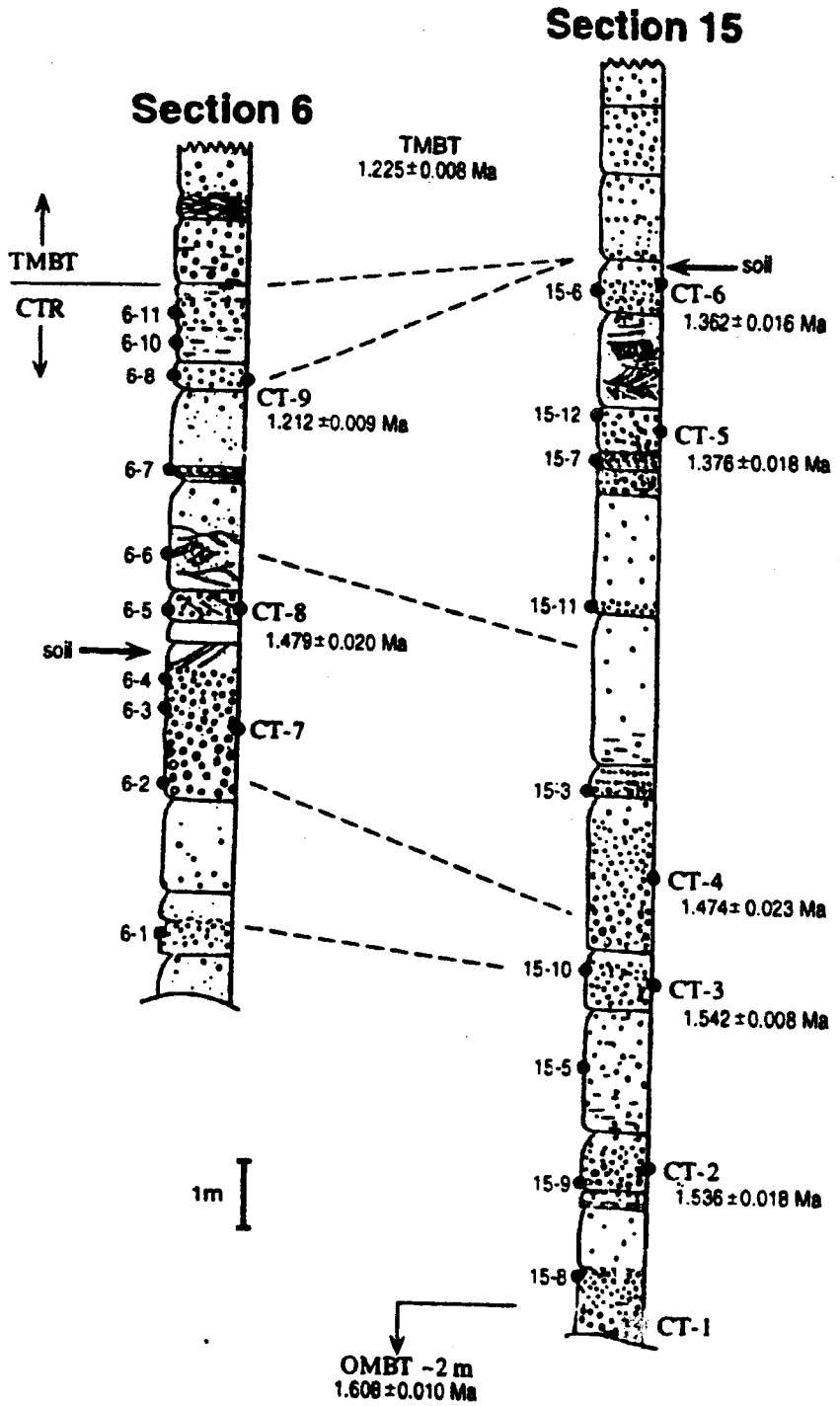

Figure 4. Composite stratigraphic column showing $^{40}Ar/^{39}Ar$ dates obtained in this study relative to the stratigraphic position of Cerro Toledo Rhyolite (CTR) tephra samples. Dashed lines between sections indicate correlated units. Arrows indicate soil horizons. Unit numbers as defined by Stix (1989). All data from the Australian National University. TMBT is Tshirege Member Bandelier Tuff; OMBT is Otowi Member Bandelier Tuff.

1.37, and 1.21 Ma (Fig. 5). There is a regular progression of decreasing age with higher stratigraphic level, with the exception of the apparent ≈150 k.y. gap between samples CT-6 and CT-5, which, as discussed below, may be material loss to erosion. The new dates indicate that the main Cerro Toledo Rhyolite eruptive activity (as recorded by the large pyroclastic pumice units sampled) occurred throughout the ≈380 k.y. interval between the Otowi Member and Tshirege Member, and that Cerro Toledo Rhyolite tephra eruptions occurred in distinct pulses ca. 1.54, 1.48, 1.37, and 1.21 Ma (Fig. 5).

The age of sample CT-3 is somewhat problematic. The isochron age of 1.451 ± 0.022 Ma suggests the presence of significant excess argon (Fig. 2), which is not evident for any of the other tephra samples analyzed. On the basis of geochemistry, CT-3 appears to group with samples CT-4, CT-7, and CT-8 (Spell et al., 1996), which are dated here as ca. 1.475 Ma, suggesting a similar age for CT-3. However, neither CT-4 nor CT-8 show signs of excess argon (Fig. 2). Thus, we suggest that the weighted mean age of 1.542 ± 0.008 Ma is preferable due to the very low spread in radiogenic yield among the analyses defining the isochron, but this age is somewhat uncertain.

For samples CT-4 and CT-7, feldspars are dominantly plagioclase and the samples are nearly aphyric, so both plagioclase and sanidine crystals were analyzed. Even though radiogenic yields as high as ≈81% were obtained for the plagioclase analyses, the data generally are discordant with coexisting sanidine and with stratigraphic relations, although precision is often poor enough that ages overlap at 2σ. Sample CT-4 is a good example of this problem because 6 sanidine ages form a coherent group, whereas 10 plagioclase analyses are scattered to both older and, dominantly, younger ages (Table 3). Excess argon could be invoked as an explanation for the older ages because this would affect plagioclase more than sanidine because of the lower K contents of plagioclase. However, the CT-4 sanidine isochron does not indicate the presence of excess argon. All mineral separates analyzed appeared pristine under the binocular microscope, although unrecognized micrometre-scale alteration cannot be ruled out. Kelley et al. (1994) noted that ultraviolet laser analysis of fractured and/or altered areas in otherwise pristine plagioclase yielded younger ages and suggested that these lowered ages were from alteration products (clays and K-feldspar). A significant correlation between radiogenic yield and age that might be expected from such a mechanism is not seen. However, this might expected for laser fusion analyses, because the intensity and duration of fusion of individual crys-

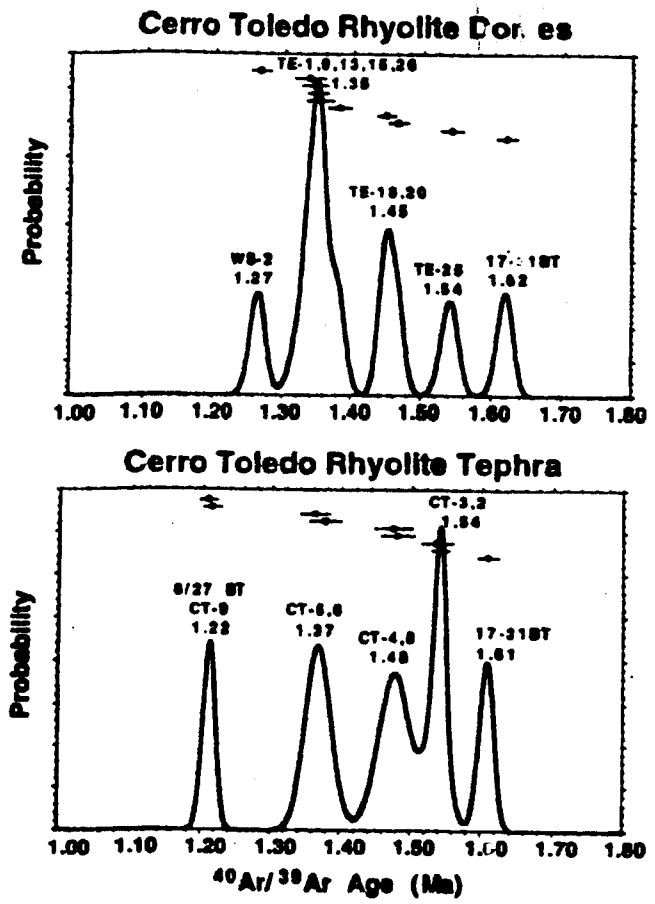

Figure 5. Probability distribution diagram illustrating eruptive periodicity during the interval between the Bandelier tuffs. Sample ages and standard deviations used are preferred $^{40}Ar/^{39}Ar$ ages and associated errors from Tables 1 and 2. Modes and samples defining modes are indicated. Cerro Toledo Rhyolite dome samples (upper diagram) analyzed at the University of Houston; tephra samples analyzed at the Australian National University (lower diagram).

tals vary resulting in varying degrees of degassing. The varying amounts of degassing may mask any possible correlation between radiogenic yield and age that may exist. In general, our experience is that total fusion plagioclase ages may not be reliable and should be interpreted with caution (cf. Pringle et al., 1992).

The distinctly more heterogeneous age population from sample CT-1, immediately above the Otowi Member makes estimation of its age somewhat problematic. These analyses fail to define an isochron, however; the mean age of these data of 1.653 ± 0.032 Ma is indistinguishable from that of the Otowi Member. The youngest $^{40}Ar/^{39}Ar$ age obtained for CT-1, 1.593 ± 0.009 Ma (Table 3), may represent this samples eruptive age, although this cannot be confirmed with certainty from the dataset. An age of ca. 1.59 Ma is consistent with the stratigraphy, which shows that CT-1 must be older than the Otowi Member (1.608 ± 0.010 Ma) and younger than CT-2 (1.536 ± 0.018 Ma) (Fig. 4, Table 1).

The observation that CT-9 yields an age identical to that of the overlying Tshirege Member (Table 1) suggests that significant volcanism was occurring immediately prior to the cataclysmic Tshirege Member eruption and collapse of the Valles caldera. These precursor eruptions resulted in deposition of ≈1 m of tephra in the sections we studied (Fig. 4), and the geochemistry of CT-9, which is identical to that of the first erupted material of the Tshirege Member (Spell et al., 1996), suggests that these eruptions were tapping the same magma chamber. These observations also allow that CT-9 records an early pulse of the Tshirege Member Plinian eruption.

The new $^{40}Ar/^{39}Ar$ dates place significant chronological constraints on a magma chamber recharge event (Stix and Gorton, 1993) recorded in samples stratigraphically equivalent with units between our samples 17-31 (Otowi Member) and CT-2. Ages of 1.608 ± 0.010 Ma (Otowi Member) and 1.536 ± 0.018 Ma (CT-2) suggest that this event occurred within ≈70 k.y. of eruption of the Otowi Member of the Bandelier Tuff and collapse of the Toledo caldera.

Cerro Toledo Rhyolite Domes

Of the nine domes dated [illegible] study, six have been previously dated by the K-Ar method (Izett et al., 1981; Stix et al., 1988; Table 2). The new $^{40}Ar/^{39}Ar$ ages are generally consistent with the previously reported ages with the exception that some are slightly older. Cerro Toledo Rhyolite dome samples WS-2, TE-1, TE-20, and TE-25 yield $^{40}Ar/^{39}Ar$ ages similar to previous K-Ar ages (Tables 1 and 2) (Izett et al., 1981; Stix et al., 1988). Sample TE-15 from the Turkey Ridge dome as well as TE-26 from Cerro Trasquilar, however, have significantly older $^{40}Ar/^{39}Ar$ ages than previous K-Ar ages (Table 2). These older ages probably reflect incomplete degassing of radiogenic argon during K-Ar dating (Webb and McDougall, 1967; McDowell, 1983).

Despite being the most contaminated unit dated in this study, having xenocrysts as old as ca. 105 Ma, Warm Springs dome gave a $^{40}Ar/^{39}Ar$ age indistinguishable from the previous K-Ar age (1.265 ± 0.011 Ma vs. 1.25 ± 0.04 Ma, respectively) (Tables 2 and 3). An integrated age (weighted by amount of ^{39}Ar per analysis) of 3.61 ± 0.018 Ma can be calculated from the $^{40}Ar/^{39}Ar$ analyses in Table 3. It is common for $^{40}Ar/^{39}Ar$ dates to be up to ≈10% older (as is the case here for TE-15) than K-Ar dates on sanidine due to incomplete extraction of radiogenic argon during K-Ar analysis (Webb and McDougall, 1967; McDowell, 1983). If the 25 crystals dated from this sample are representative of the crystal population, then the K-Ar age of 1.25 Ma is ≈65% younger, which would be unusual. This suggests that the xenocrystic component is overrepresented in our analytical data.

The $^{40}Ar/^{39}Ar$ age of 1.343 ± 0.015 Ma obtained for Turkey Ridge dome (Table 2) is 8.3% older than the previous K-Ar age of 1.24 ± 0.03 Ma reported by Stix et al. (1988). The Unnamed dome gives a $^{40}Ar/^{39}Ar$ age of 1.348 ± 0.010 Ma, indistinguishable from the previous K-Ar age of 1.33 ± 0.02 Ma (Table 2). Cerro Trasquilar, sample TE-26, gave a $^{40}Ar/^{39}Ar$ age of 1.359 ± 0.012 Ma, which is 7.0% older than the previously reported age of 1.27 ± 0.02 Ma (Table 2).

Sample TE-20, from Los Posos East dome, with the exception of tephra sample C[illegible] cussed above, the only sample dated [illegible]

that shows evidence for significant excess ^{40}Ar with an indicated initial $^{40}Ar/^{36}Ar$ of 402 ± 33 (Fig. 2). Because most of these analyses are highly radiogenic, the mean and weighted mean ages (calculated assuming an atmospheric initial argon composition) are only ≈2% older (contrasting with CT-3 analyses that are less radiogenic, resulting in mean and weighted mean ages ≈6% older). Because the TE-20 isochron is defined by a large number of analyses (n = 20) with a reasonable spread in radiogenic yield, we take the isochron age as the best estimate of the eruptive age of the Los Posos East dome. The isochron ages of TE-20 (1.446 ± 0.009 Ma) and CT-3 (1.451 ± 0.022 Ma) are indistinguishable, suggesting that CT-3 tephra is the Plinian phase of the eruption that produced the Los Posos East dome. However, these two units are distinct geochemically, suggesting that they are unrelated (Spell et al., 1996).

The last Cerro Toledo Rhyolite dome we dated that was previously dated by the K-Ar method is Los Posos West (sample TE-25). Although the $^{40}Ar/^{39}Ar$ isochron date of 1.540 ± 0.012 Ma is within error of the previous 1.50 ± 0.05 Ma date, it is ≈2.7% older and significantly more precise (Table 2).

Cerro Toledo Rhyolite domes dated during this study are within the Toledo embayment with the exception of Warm Springs dome, Cerro Trasquilar, and possibly the Los Posos domes (Fig. 1). There is no apparent regular progression of ages with geographic locality within what remains of the Toledo caldera. Two samples of Sierra de Toledo, a previously undated dome, yield ages of 1.336 ± 0.018 Ma (TE-9) and 1.379 ± 0.012 Ma (TE-13), which are 3.2% different and distinguishable at the 1σ confidence level. The Sierra de Toledo dome may be a composite unit produced by multiple eruptions. Note that Turkey Ridge (1.343 ± 0.015 Ma) and the Sierra de Toledo dome form a continuous morphological feature and thus may represent a single eruptive event between ≈1.34 and 1.38 Ma.

The most obvious aspect of the $^{40}Ar/^{39}Ar$ dates on Cerro Toledo Rhyolite domes is the fact that five of the nine samples dated fall in an interval between the dates on the two Sierra de Toledo samples TE-9 and TE-13. This is also an interval of time during which two of the Cerro Toledo Rhyolite tephra samples (CT-5, CT-6) were erupted (Fig. 2, Table 1). The previously undated Indian Point dome gave a $^{40}Ar/^{39}Ar$ age of 1.463 ± 0.011 Ma. As with Cerro Toledo Rhyolite tephra samples, the domes dated were erupted during discrete periods separated by longer quiescent intervals. Eruptions occurred at 1.54, 1.45, 1.38–1.34, and 1.27 Ma. Quiescent intervals of 70–80 k.y. separate these volcanic periods.

Correlations Between Cerro Toledo Rhyolite Tephra and Domes

Initial speculations on correlations between Cerro Toledo Rhyolite tephra and domes were made by Heiken et al. (1986), who suggested that the Los Posos (East Los Posos in particular) domes or the Cerro Toledo domes corresponded to tephra units that include our samples CT-1, CT-2, CT-3, CT-4, and CT-7 in stratigraphic levels 5 through 23 (Table 1). Heiken et al. (1986) also indicated that stratigraphic levels 26 through 41 (Table 1) (CT-8, CT-5, CT-6, and CT-9) correlate with Pinnacle Peak, which was not dated in this study.

Stix et al. (1988) discussed correlations between Cerro Toledo Rhyolite tephra and domes based on the more detailed geochemistry and geochronology available at that time. They suggested that the Los Posos domes (Fig. 1) with K-Ar ages of 1.47–1.50 Ma (Heiken et al., 1986) correlate with tephra units corresponding to our samples CT-3, CT-4, and CT-7, which are dated here as 1.47 to 1.54 Ma (Table 1). Stratigraphic units, below which our sample CT-8 lies, were suggested to correlate with the Turkey Ridge domes (dated as 1.24 ± 0.03 Ma by Heiken et al., 1986). The Southeast Rhyolite dome, Pinnacle Peak, Warm Springs dome, and Cerro Trasquilar were suggested to correlate with tephra units corresponding to our samples CT-6 through CT-9 (Stix et al., 1988).

The $^{40}Ar/^{39}Ar$ ages reported here (Tables 1 and 2) allow these correlations to be tested. Both Cerro Toledo Rhyolite tephra and dome samples record periodic volcanic activity and have similar timing for these eruptive periods. Eruptive activity is recorded in Cerro Toledo Rhyolite tephra at 1.54, 1.48, 1.37, and 1.21 Ma. A similar timing of eruptive episodes is defined by the Cerro Toledo Rhyolite dome samples dated in this study as 1.54, 1.45, 1.38–1.34, and 1.27 Ma (Fig. 5).

Tephra samples CT-2 and CT-3 (1.536 ± 0.018 and 1.542 ± 0.008 Ma, respectively) from near the base of the section yield ages identical to those obtained on Los Posos West dome sample TE-25 (1.540 ± 0.012 Ma). This result confirms the suggestions of Heiken et al. (1986) and Stix et al. (1988) that CT-2 and CT-2 correlate with the Los Posos West dome, but shows that Los Posos East (see below) does not correlate to these stratigraphic levels in the tephra and also shows that CT-4 and CT-7 are not correlative with Los Posos West (Fig. 5).

Farther upsection, tephra samples CT-4 and CT-8 (1.474 ± 0.023 and 1.479 ± 0.020 Ma, respectively) correlate with the Indian Point and Los Posos East domes samples TE-18 and TE-20 (1.463 ± 0.011 and 1.446 ± 0.009 Ma, respectively), although there is a suggestion that Los Posos East may be slightly younger than these Cerro Toledo Rhyolite tephra samples. Heiken et al. (1986) and Stix et al. (1988) suggested the correlation between CT-4 and Los Posos East which our $^{40}Ar/^{39}Ar$ dates confirm. Stix et al. (1988) correlated a section of Cerro Toledo Rhyolite tephra with the Turkey Ridge dome. Our CT-8 sample lies below this. The 1.479 Ma $^{40}Ar/^{39}Ar$ age for CT-8 and the 1.343 Ma $^{40}Ar/^{39}Ar$ date on TE-15, from Turkey Ridge, do not support this correlation.

Tephra samples CT-5 and CT-6 (1.376 ± 0.018 and 1.362 ± 0.016, respectively) correlate temporally with a large group of samples from Sierra de Toledo, Cerro Trasquilar, Unnamed dome, and Turkey Ridge, samples TE-13 (1.379 ± 0.012 Ma), TE-26 (1.351 ± 0.015 Ma), TE-1 (1.348 ± 0.010 Ma), TE-15 (1.343 ± 0.015 Ma), and TE-9 (1.336 ± 0.018 Ma). Stix et al. (1988) suggested the correlation between CT-6 and the Warm Springs and Cerro Trasquilar domes, which is supported by our data.

There is no correlative tephra for the Warm Springs dome (WS-2, 1.265 ± 0.011 Ma). Stix et al. (1988) indicated a correlation between tephra corresponding to CT-6 and CT-9 with the Warm Springs dome. Our data show that CT-6 is significantly older and CT-9 significantly younger than the Warm Springs dome (Tables 1 and 2). There is no Plinian pumice fall unit within the Cerro Toledo Rhyolite tephra sections we sampled—stratigraphically between CT-6 and CT-9—that might represent the initial phase of the eruption producing the Warm Springs dome.

At the top of the Cerro Toledo Rhyolite stratigraphic section, tephra sample CT-9 (1.212 ± 0.009 Ma) does not correlate with any domes dated in this study; however, it has an age indistinguishable from that of the Tshirege Member (1.225 ± 0.008 Ma). This is consistent with the geochemistry of CT-9, which is indistinguishable from the overlying Tshirege Member Plinian pumice (Spell et al., 1996).

SUMMARY

The Cerro Toledo Rhyolites record volcanism during the ≈380 k.y. interval between two caldera-forming eruptions; the Tshirege and Otowi members of the Bandelier Tuff in the Jemez Volcanic Field. They contain important information about the evolution of this large crustal silicic magma system during the transition from and to caldera collapse events; this study provides the good chronological control which is essential for interpreting such data.

$^{40}Ar/^{39}Ar$ dating of nine major pumice fall units within the Cerro Toledo Rhyolite tephra, which may record the inception of significant dome extrusion events within the Toledo caldera,

yields a detailed chronology of eruptive activity; seven of these units have reliable and stratigraphically consistent ages. With a few exceptions, reliable sanidine isochrons were obtained from multiple laser fusions of individual phenocrysts. For some sparsely porphyritic samples in which the dominant feldspar is plagioclase, this phase was analyzed. Plagioclase dates were generally of poor precision, discordant with coexisting sanidine, and inconsistent with stratigraphic constraints. The dates obtained suggest that Cerro Toledo Rhyolite Plinian pumice fall eruptions occurred throughout the interval between the Bandelier tuffs (ca. 1.61–1.23 Ma), but that sequences of these eruptions occurred in pulses at ca. 1.54, 1.48, 1.37, and 1.22 Ma. $^{40}Ar/^{39}Ar$ dates indicate that Cerro Toledo Rhyolite rhyolite domes were produced at 1.54, 1.45, 1.38–1.34, and 1.27 Ma, and show that many can be correlated chronologically with the tephra sequence. The oldest and youngest Cerro Toledo Rhyolite tephra are indistinguishable in age from the Otowi Member and Tshirege Member, respectively, and thus their geochemistry may provide insight into the final products of the Otowi Member magma chamber and the earliest phases of the Tshirege Member magma chamber.

The eruptive chronology provided by this study, when combined with geochemical and isotopic data (Stix and Gorton, 1993; Spell et al., 1996) should significantly enhance our understanding of the evolution of the Bandelier silicic magma system. For example, evidence for a magma chamber recharge event recorded in Cerro Toledo Rhyolite tephra immediately above the Otowi Member (Stix and Gorton, 1993), combined with stratigraphic and age constraints, indicate that this occurred within ≈70 k.y. of caldera collapse.

ACKNOWLEDGMENTS

The Baca Land and Cattle Company allowed us access to their land for sample collection. We thank P. Kyle for collaboration on Jemez Volcanic Field studies and J. Stix for sharing his knowledge of stratigraphic relationships in the Cerro Toledo Rhyolite tephra. J. Wolff supplied samples from the Bandelier Tuff. J. Mya and S. Paxton assisted with mineral separations and R. Maier provided technical support during the intralaboratory calibration and K-Ar analyses of our Fish Canyon Tuff sanidine separate 92-176 at the Australian National University. Neutron irradiations were facilitated by the Australian Institute of Nuclear Science and Engineering and the Australian Nuclear Science and Technology Organization and by the Department of Energy and the Nuclear Science Center at Texas A&M University. Establishment of the University Houston Thermochronology Laboratory was funded by National Science Foundation grant EAR-9219905 to P. Copeland. An early version of the manuscript benefited from comments by P. Kyle, J. Stix, and J. Wolff. Reviews by J. Gardner and W. McIntosh helped improve and refine the manuscript.

REFERENCES CITED

Bailey, R. A., Smith, R. L., and Ross, C. S., 1969, Stratigraphic nomenclature of volcanic rocks in the Jemez Mountains, New Mexico: U.S. Geological Survey Bulletin 1274-P, p. 1–19.

Balsley, S. D., 1988, The petrology and geochemistry of the Tshirege Member of the Bandelier Tuff, Jemez Mountains Volcanic Field, New Mexico, U.S.A. [Master's thesis]: Arlington, University of Texas at Arlington, 188 p.

Bogaard, P. v., 1995, $^{40}Ar/^{39}Ar$ ages of sanidine phenocrysts from Laacher See Tephra (12,900 yr BP): Chronostratigraphic and petrological significance: Earth and Planetary Science Letters, v. 133, p. 163–174.

Cebula, G. T., Kunk, M. J., Mehnert, H. H., Naeser, C. W., Obradovich, J. D., and Sutter, J. F., 1986, The Fish Canyon Tuff, a potential standard for the $^{40}Ar/^{39}Ar$ and fission-track dating methods: Terra Cognita, Abstracts, v. 6, p. 139.

Christensen, J. N., and DePaolo, D. J., 1993, Time scales of large volume silicic magma systems: Sr isotopic systematics of phenocrysts and glass from the Bishop Tuff, Long Valley, California: Contributions to Mineralogy and Petrology, v. 113, p. 100–114.

Dalrymple, G. B., and Lanphere, M. A., 1971, $^{40}Ar/^{39}Ar$ technique of K-Ar dating: A comparison with the conventional technique: Earth and Planetary Science Letters, v. 12, p. 300–308.

Davies, G. R., Halliday, A. N., Mahood, G. A., and Hall, C. M., 1994, Isotopic constraints on the production rates, crystallization histories, and residence times of precaldera silicic magmas, Long Valley, California: Earth and Planetary Science Letters, v. 125, p. 17–37.

Deino, A. L., and Potts, R., 1990, Single-crystal $^{40}Ar/^{39}Ar$ dating of the Olorgesailie Formation, southern Kenya rift: Journal of Geophysical Research, v. 95, p. 8453–8470.

Doell, R. R., and Dalrymple, G. B., 1966, Geomagnetic polarity epochs: A new polarity event and the age of the Brunhes-Matuyama boundary: Science, v. 152, p. 1060–1061.

Doell, R. R., Dalrymple, G. B., Smith, R. L., and Bailey, R. A., 1968, Paleomagnetism, potassium-argon ages, and geology of rhyolites and associated rocks of the Valles Caldera, New Mexico: Geological Society of America Memoir 116, p. 211–248.

Gardner, J. N., and Goff, F., 1984, Potassium-argon dates from the Jemez Volcanic Field: Implications for tectonic activity in the north-central Rio Grande rift: New Mexico Geological Society Field Conference Guidebook 35, p. 75–81.

Gardner, J. N., Goff, F., Garcia, S., and Hagan, R. C., 1986, Stratigraphic relations and lithologic variations in the Jemez Volcanic Field, New Mexico: Journal of Geophysical Research, v. 91, p. 1763–1778.

Griggs, R. L., 1964, Geology and ground water resources of the Los Alamos area, New Mexico: U.S. Geological Survey Water-Supply Paper 1753, 107 p.

Halliday, A. N., Mahood, G. A., Holden, P., Metz, J. M., Dempster, T. J., and Davidson, J. P., 1989, Evidence for long residence times of rhyolitic magma in the Long Valley magmatic system: The isotopic record in precaldera lavas of Glass Mountain: Earth and Planetary Science Letters, v. 94, p. 274–290.

Heiken, G., Goff, F., Stix, J., Tamanyu, G., Shafiqullah, M., Garcia, S., and Hagan, R., 1986, Intracaldera volcanic activity, Toledo Caldera and Embayment, Jemez Mountains, New Mexico: Journal of Geophysical Research, v. 91, p. 1799–1815.

Hildreth, W., 1981, Gradients in silicic magma chambers: Implications for lithospheric magmatism: Journal of Geophysical Research, v. 86, p. 10153–10192.

Huppert, H. E., and Sparks, R. S. J., 1988, The generation of granitic magmas by intrusion of basalt into continental crust: Journal of Petrology, v. 29, p. 599–624.

Hurford, A. J., and Hammerschmidt, K., 1985, $^{40}Ar/^{39}Ar$ and K-Ar dating of the Bishop and Fish Canyon tuffs: Calibration ages for fission-track dating standards: Chemical Geology (Isotope Geoscience Section), v. 58, p. 23–32.

Izett, G. A., and Obradovich, J. D., 1994, $^{40}Ar/^{39}Ar$ age constraints for the Jaramillo Normal Subchron and the Matuyama-Brunhes geomagnetic boundary: Journal of Geophysical Research, v. [illegible], p. 2925–2934.

Izett, G. A., Obradovich, J. D., Naeser, C. W., [illegible] Potassium-argon and fission-track [illegible] rhyolite tephra in the Jemez Mountains, New Mexico: U.S. Geological Survey Professional Paper 1199-[illegible]

Kelley, S. P., Arnaud, N. O., and Turner, S. P., 1994, High spatial resolution $^{40}Ar/^{39}Ar$ investigations using an ultra-violet laser probe extraction technique: Geochimica et Cosmochimica Acta, v. [illegible], p. 3519–3525.

Kuentz, D. C., 1986, The Otowi Member of the Bandelier Tuff: A study of the petrology, petrography, and geochemistry of [illegible] silicic eruption, Jemez Mountains, New Mexico [Master's thesis]: Arlington, Texas, University of Texas, 168 p.

Lipman, P. W., 1984, The roots of ash flow calderas in western North America: Windows into the tops of granitic batholiths: Journal of Geophysical Research, v. 89, p. 8801–8841.

McDowell, F. W., 1983, K-Ar dating: Incomplete [illegible] of radiogenic argon from alkali feldspar: Chemical Geology (Isotope Geoscience Section), v. 1, p. 119–126.

Pringle, M. S., McWilliams, M., Houghton, B. F., Lanphere, M. A., and Wilson, C. J. N., 1992, $^{40}Ar/^{39}Ar$ dating of Quaternary feldspar: Examples from the Taupo Volcanic Zone, New Zealand: Geology, v. 20, p. 531–534.

Reneau, S. L., Gardner, J. N., and Forman, S. L., 1996, New evidence for the age of the youngest eruptions in the Valles caldera, New Mexico: Geology, v. 24, p. 7–10.

Self, S., Goff, F., Gardner, J. N., Wright, J. V., and Kite, W. M., 1986, Explosive rhyolitic volcanism in the Jemez Mountains: Vent locations, caldera development, and relation to regional structure: Journal of Geophysical Research, v. 91, p. 1779–1798.

Smith, R. L., 1979, Ash-flow magmatism: Geological Society of America Special Paper 180, p. 5–27.

Smith, R. L., and Bailey, R. A., 1968, Resurgent cauldrons: Geological Society of America Memoir 116, p. 613–662.

Smith, R. L., Bailey, R. A., and Ross, C. S., 1970, Geologic map of the Jemez Mountains, New Mexico: U.S. Geological Survey Miscellaneous Geologic Investigation Map I-571, scale 1:125 000.

Spell, T. L., and Harrison, T. M., 1993, $^{40}Ar/^{39}Ar$ geochronology of post-Valles Caldera rhyolites, Jemez volcanic field, New Mexico: Journal of Geophysical Research, v. 98, p. 8031–8051.

Spell, T. L., and Kyle, P. R., 1989, Petrogenesis of Valle Grande Member rhyolites, Valles Caldera, New Mexico: Implications for evolution of the Jemez Mountains magmatic system: Journal of Geophysical Research, v. 94, p. 10379–10396.

Spell, T. L., Harrison, T. M., and Wolff, J. A., 1990, $^{40}Ar/^{39}Ar$ dating of the Bandelier Tuff and San Diego Canyon ignimbrites: Temporal constraints on magmatic evolution: Journal of Volcanology and Geothermal Research, v. 43, p. 175–193.

Spell, T. L., Kyle, P. R., and Baker, J., 1996, Geochronology and geochemistry of the Cerro Toledo Rhyolite: New Mexico Geological Society, 47th Annual Field Conference Guidebook, p. 263–268.

Steiger, R. H., and Jager, E., 1977, Subcommission on geochronology: Convention on the use of decay constants in geo- and cosmochronology: Earth and Planetary Science Letters, v. 36, p. 359–362.

Steven, T. A., Mehnert, H. H., and Obradovich, J. D., 1967, Age of volcanic activity in the San Juan Mountains, Colorado: U.S. Geological Survey Professional Paper 575-D, p. 47–55.

Stix, J. F., 1989, Physical and chemical fractionation processes in subaerial and subaqueous pyroclastic rocks [Ph.D. dissert.]: Toronto, Ontario, University of Toronto, 365 p.

Stix, J. F., and Gorton, M. P., 1993, Replenishment and crystallization in epicontinental silicic magma chambers: Evidence from the Bandelier magmatic system: Journal of Volcanology and Geothermal Research, v. 55, p. 201–215.

Stix, J., Goff, F., Gorton, M. P., Heiken, G., and Garcia, S. R., 1988, Restoration of compositional zonation in the Bandelier silicic magma chamber between two caldera-forming eruptions: Geochemistry and origin of the Cerro Toledo Rhyolite: Journal of Geophysical Research, v. 93, p. 6129–6147.

Turbeville, B. N., and Self, S., 1988, San Diego Canyon ignimbrites: Pre-Bandelier Tuff explosive rhyolitic volcanism in the Jemez Mountains, New Mexico: Journal of Geophysical Research, v. 93, p. 6148–6156.

Webb, A. W., and McDougall, I., 1967, A comparison of mineral and whole rock potassium-argon ages of Tertiary volcanics from Central Queensland, Australia: Earth and Planetary Science Letters, v. 3, p. 41–47.

York, D., 1969, Least squares fitting of a straight line with correlated errors: Earth and Planetary Science Letters, v. 5, p. 320–324.

Young, H. D., 1962, Statistical treatment of experimental data: New York, McGraw-Hill, 172 p.

Manuscript Received by the Society June 9, 1995
Revised Manuscript Received by the Society April 4, [illegible]
Manuscript Accepted May 7, 1996